Level structure of ^{30}S and its importance in the ^{26}Si(α,p)^{29}P and ^{29}P(p,γ)^{30}S reaction rates

S. Almaraz-Calderon *et al.*

Phys. Rev. C **86**, 065805 — Published 20 December 2012

DOI: 10.1103/PhysRevC.86.065805

THE LEVEL STRUCTURE OF ^{30}S AND ITS IMPORTANCE IN THE ^{26}Si(α,p)^{29}P and ^{29}P(p,γ)^{30}S REACTION RATES.

S. Almaraz-Calderon,* W. P. Tan, A. Aprahamian, M. Beard, G. P. A. Berg, B. Bucher, M. Couder, J. Görres, S. O'Brien, D. Patel, A. Roberts, K. Sault, and M. Wiescher†
Department of Physics, University of Notre Dame, Notre Dame, IN 46556, USA

C. R. Brune and T. N. Massey
Department of Physics and Astronomy, Ohio University, Athens, OH 45701, USA

K. Fujita, K. Hatanaka, D. Ishiwaka, H. Matsubara, H. Okamura, H. J. Ong, Y. Sakemi, Y. Shimizu,‡ T. Suzuki, Y. Tameshige,§ A. Tamii, and J. Zenihiro
Research Center for Nuclear Physics, Osaka University, Ibaraki, Osaka 560-0047, Japan

T. Kubo, Y. Namiki, Y. Ohkuma, Y. Shimbara, S. Suzuki, R. Watanabe, and R. Yamada
Graduate School of Science and Technology, Niigata University, Nishi-ku, Niigata 950-2181, Japan

T. Adachi¶ and Y. Fujita
Department of Physics, Osaka University, Toyonaka, Osaka 560-0043, Japan

H. Fujita
School of Physics, University of the Witwatersrand, PO Wits, Johannesburg 2050, South Africa

M. Dozono and T. Wakasa
Department of Physics, Kyushu University, Fukuoka 812-8581, Japan
(Dated: October 29, 2012)

The level structure of ^{30}S was studied via the ^{28}Si(^{3}He,n) and ^{32}S(p,t) reactions at the Nuclear Science Laboratory (NSL) of the University of Notre Dame and the Research Center for Nuclear Physics (RCNP) of the University of Osaka, Japan. Important experimental information on the energy levels, decay branching ratios and tentative spin assignments are extracted to calculate the reaction rates for ^{29}P(p,γ)^{30}S and ^{26}Si(α,p)^{29}P, which play a critical role for reaction flow in explosive hydrogen burning.

PACS numbers: 21.10.Ma, 24.30.-v, 26.30.-k, 26.50.+x, 27.30.+t.

* salmaraz@nd.edu; Present address: Physics Division, Argonne National Laboratory, Argonne, IL 60439, USA
† mwiesche@nd.edu
‡ Present address: Center for Nuclear Study, University of Tokyo, Wako, Saitama 351-0198, Japan
§ Present address: Office for Development of Proton Therapy Center, Regional Health Services Division, Department of Health and Welfare Fukui Prefectural Government, Fukui City, Fukui Prefecture 910-0846, Japan
¶ Present Address: Research Center for Electron Photon Science, Tohoku University, Taihaku-ku, Sendai, Miyagi 982-0826, Japan

I. INTRODUCTION

The level structure of ^{30}S is key to understanding the αp- and the *rp*-processes since it plays a crucial role in the calculation of the ^{29}P(p,γ) and ^{26}Si(α,p) reaction rates. These two reaction rates are by themselves important to understanding explosive hydrogen burning environments like novae and X-ray bursts.

Thermonuclear runaway processes in accreting binary star systems like Novae and X-ray bursts are driven by the *rp*- and αp-processes along the proton-rich side of the chart of nuclides transferring nuclear material from the Hot CNO cycle up to mass A $\sim$ 40 [1–3]. For lower temperature environments such as anticipated for Ne-novae [4], the reaction flow above Z = 10 is driven by the classical *rp-process*, characterized by a sequence of proton capture reactions and β-decays transforming material from the Ne, Mg mass region into the Si, S mass region [2, 5]. The reaction rates associated with the endpoint of the hydrogen burning in Ne-novae are of particular importance for the analysis of the abundances in nova ejecta [6].

The ^{29}P(p,γ) reaction rate is therefore of great interest for constraining nova models. The study of presolar grains in the laboratory has been used as a tool for identification of parent stellar sources based on the isotopic signatures [7]. Some of these grains have been identified to be of nova origin [8]. The ^{29}Si and ^{30}Si abundances are good indicators of the peak temperatures achieved in the explosions and of the dominant nuclear paths followed in the course of a thermonuclear runaway leaving a clear imprint on the overall composition of the ejecta [9]. In order to interpret the Si abundance measurements, the thermonuclear reaction rates affecting Si production in novae are needed. One of these relevant reaction rates is the ^{29}P(p,γ)^{30}S reaction rate. This reaction rate affects the direct flow away from ^{29}Si (the product of the β^+-decay of ^{29}P) and towards ^{30}Si via the reaction chain ^{29}P(p,γ)^{30}S(β^+)^{30}P(β^+)^{30}Si [10]. A sensitivity study performed by Iliadis *et al.* [6], found that ^{29,30}Si abundances change by about a factor of 3 when the ^{29}P(p,γ)^{30}S reaction was varied within the prescribed limits.

In higher temperature environments such as those anticipated for the atmosphere of accreting neutron stars [1], the thermonuclear runaway is driven by the *αp-process*, by-passing the β^+-decay waiting point nuclei of the *rp-process* ^{22}Mg, ^{26}Si, ^{30}S and ^{34}Ar [3]. The *αp-process* is triggered by the α-capture on ^{18}Ne in the Hot CNO cycle and proceeds via the reaction sequence ^{18}Ne(α,p)^{21}Na(p,γ)^{22}Mg(α,p) ^{25}Al(p,γ)^{26}Si(α,p)^{29}P(p,γ)^{30}S(α,p)^{33}Cl(p,γ)^{34}Ar(α,p) ^{37}K(p,γ)^{38}Ca(α,p). Above Z = 20 the Coulomb barrier reduces the α-capture reaction rates which leads to a termination of the *αp-process*. The thermonuclear runaway above Z = 20 is predicted to be entirely driven by the *rp-process*, as a sequence of proton-capture reactions and β-decay processes. Two of the relevant reaction links are the ^{26}Si(α,p)^{29}P reaction followed by the ^{29}P(p,γ)^{30}S radiative capture process which take place through resonant states of the compound nucleus ^{30}S, making their reaction rates very sensitive to the level structure of the relevant resonances in ^{30}S. The ^{26}Si(α,p) reaction rate has been identified for playing a particularly important role in understanding the observed double-peaked structure in the bolometric luminosity of X-ray bursts. The observed peak separation of 4 - 7 seconds [11–13] has been interpreted as a delay in the energy generation and therefore temporary reduction in the X-ray flux due to the impedance associated with the ^{26}Si(α,p)^{29}P and ^{34}Ar(α,p)^{33}Cl reactions [14].

The reaction rate predictions for ^{29}P(p,γ) and ^{26}Si(α,p) are uncertain due to the limited information about the level structure and level characteristics above the proton threshold and the alpha threshold, respectively.

In order to calculate the ^{29}P(p,γ) rate, experimental information on the unbound levels of ^{30}S above the proton threshold at E_x = 4.399 MeV up to the alpha threshold is required. By studying the analog levels in the A = 30 isobaric chain, Wiescher and Görres [15] as well as Iliadis *et al.* [16], concluded that the ^{29}P(p,γ) reaction rate at nova temperatures is dominated by two low-lying 3^+ and 2^+ resonances. However, there is no firm experimental evidence for the existence of these 3^+ and 2^+ levels in ^{30}S despite many experimental efforts [17–21]. Using the isobaric-multiplet mass equation, Iliadis *et al.* [16] estimated that the level energies should be E_x = 4.733 MeV and E_x = 4.888 MeV respectively. Recent experiments using the ^{32}S(p,t)^{30}S reaction have confirmed a 3^+ energy level at E_x = 4.699 MeV [10, 22] and showed evidence for the 2^+ resonance level at E_x = 4.814 MeV [22]. These results reduced the uncertainties in previous reaction rate predictions considerably, but the resonance strengths used for this calculation still depend on the adopted single-particle spectroscopic factors from the mirror levels in ^{30}Si [22].

The presently adopted rate of the ^{26}Si(α,p) reaction is much more poorly known. No experimental information is known about the level structure of ^{30}S above the alpha threshold at E_x = 9.343 MeV; a high level density was assumed for this excitation range and the presently used reaction rate is based on Hauser-Feshbach predictions. While this assumption has been shown to be valid for the case of the ^{22}Mg(α,p)^{25}Al reaction [23], it still depends on a limited number of natural-parity resonance states which dominate the rate. An independent evaluation of the level density and level parameters in ^{30}S is therefore necessary to confirm the Hauser-Feshbach prediction.

In this work, we studied the resonant level structure of ^{30}S via the ^{32}S(p,t) two-neutron and the ^{28}Si(^{3}He,n) two-proton transfer reactions. The main goal of the first study was to identify proton- and alpha-unbound levels in ^{30}S and determine the excitation energies with high accuracy by taking advantage of the high resolving power of the dispersion matched Grand Raiden spectrometer at RCNP, Osaka, Japan. The second measurement aimed at a study of the decay properties of these unbound states by mapping the decay-particle channels in coincidence with

the neutrons populating the respective levels. The neutron detector set-up at NSL Notre Dame had only limited Time-of-Flight (ToF) resolution because of the relatively short flight path but covered a large angle which improved the overall efficiency.

The combined data of both experiments provide new experimental information on the energies, branching ratios and tentative spin-parity assignments of several ^{30}S states up to E_x = 12 MeV that are expected to be of great importance in the calculation of the astrophysically important ^{26}Si(α,p)^{29}P and ^{29}P(p,γ)^{30}S reaction rates.

II. THE $^{32}S(p,t)$ EXPERIMENT

To investigate the proton- and alpha-unbound states in ^{30}S and to determine the excitation energies with high accuracy we performed a ^{32}S(p,t)^{30}S experiment at the Ring Cyclotron facility of the Research Center for Nuclear Physics (RCNP) at Osaka University. This measurement used the same technique as our previous studies of the ^{24}Mg(p,t)^{22}Mg reaction [24] and the ^{28}Si(p,t)^{26}Si reaction [25]. The details of the experimental technique and the data analysis are discussed extensively in these works [24, 28] and will, therefore, only be summarized briefly here.

A 98.7 MeV proton beam from the Ring Cyclotron was transported via the "fully dispersion-matched" WS beam line [29] to the target chamber of the high-resolution spectrometer Grand Raiden (GR). The proton beam impinged on a 3.38 mg/cm^2 highly enriched ($\geq$ 99 %) self-supporting ^{32}S target, sandwiched between two 250 μg/cm^2 Au layers to contain the sulfur under beam bombardment. The target itself was liquid-nitrogen cooled to allow for beam currents up to 10 nA without loss of target material due to sublimation. The target thickness translated into an energy spread of roughly 35 keV for the outgoing tritons, which dominated the final resolution at the focal plane of the GR spectrometer [28]. Fig. 1 shows a combined ^{30}S spectrum in the full range from the ground states (g.s.) up to 12.3 MeV excitation energy at spectrometer angles of -0.3° and 8.0°. For the identification and subtraction of events from ^{12}C and ^{16}O contaminants, a 1 mg/cm^2 thick ^{12}C target and a 1 mg/cm^2 thick Mylar target were used. The target contamination was low; only the ground state population of ^{14}O was identified below 2 MeV due to the ^{16}O(p,t)^{14}O background reaction on oxygen contamination trapped between the different target layers. The ground state transition of ^{12}C(p,t)^{10}C was identified just below 5.5 MeV and resulted from reactions with ^{12}C surface contamination of the target material. Higher excited states in ^{10}C and ^{14}O contributed only weakly as background to the spectra taken at the high-momentum setting.

The goal of the ^{32}S(p,t)^{30}S experiment was to investigate the nuclear structure of ^{30}S from the ground state up to 12.3 MeV excitation energy. Because of the small momentum acceptance of 5 % of GR [28] we performed measurements at two different magnetic settings in order to collect spectra over this entire energy with sufficient overlap to obtain a consistent energy calibration. The high-momentum magnetic field of B_1 = 727.1 mT covered the excitation range between 0 MeV and 7 MeV suitable for the study of resonance levels in the ^{29}P(p,γ)^{30}S reaction, while the low-momentum setting of the magnetic field B_2 = 689.7 mT covered an excitation range from 6.2 MeV to 12.3 MeV, sufficient for studying the resonance levels in the ^{26}Si(α,p)^{30}S reaction. We took each of these measurements at two different angles -0.3° and 8° with the purpose of spin-parity identification from the angle dependent reaction yields.

Calibration of ^{32}S(p,t)^{30}S spectra above the α-emission threshold was done by using the well-known low-lying states as described in Ref. [24]. The absolute calibration of the focal-plane position versus Bρ was performed by using the calibration of ^{24}Mg(p,t)^{22}Mg spectra (see Ref. [24]). Therefore, the calculated ^{30}S excitation energies are sensitive to possible uncertainties in the beam-energy. Changing the value of the beam-energy by 100 keV translates into a change in the ^{30}S excitation energies of up to 0.5 keV for states at high excitation energy.

Only the uncertainty in the x position in the focal plane is considered as statistical error in the ^{30}S excitation energies. The statistical error is calculated as the FWHM of 35 keV divided by the square root of the number of counts under the peak and is therefore strongly dependent on the statistics. As an example for a typical, small peak with 100 counts the statistical error is 3.5 keV and 0.78 keV for a large peak with 2000 events. The systematic error includes uncertainties originating from the reaction-angle determination, the mass of ^{30}S (0.5 keV), and the error resulting from the uncertainty in the beam-energy (0.5 keV). The uncertainty of 0.5 keV of the mass of ^{30}S is the sum of the uncertainty of 0.3 keV of the mass of ^{30}P [26] and the mass difference of 0.2 keV of ^{30}P and ^{30}S measured by Souin *et al.* [27]. Due to the method of angular dispersion matching [24] the scattering angle can be reconstructed with an uncertainty of 5 to 8 mrad depending on the position of the focal plane. This translates into a kinematic error of 0.1 keV at 0° scattering angle and 3.9 keV and 6.3 keV, respectively, at 8°. These three systematic errors are quadratically added to obtain the total systematic error. The systematic and statistical errors are added linearly to obtain the total error, which is quoted for the present ^{30}S excitation energies. Because of discrepancies between the resulting excitation energies in ^{30}S and the results of previous work [21] a second calibration run was performed using the ^{46}Ti(p,t)^{44}Ti reaction at a 0.92 mg/cm^2 86.1 % isotopically enriched ^{46}Ti target giving consistent results for the energy calibration of the spectra.

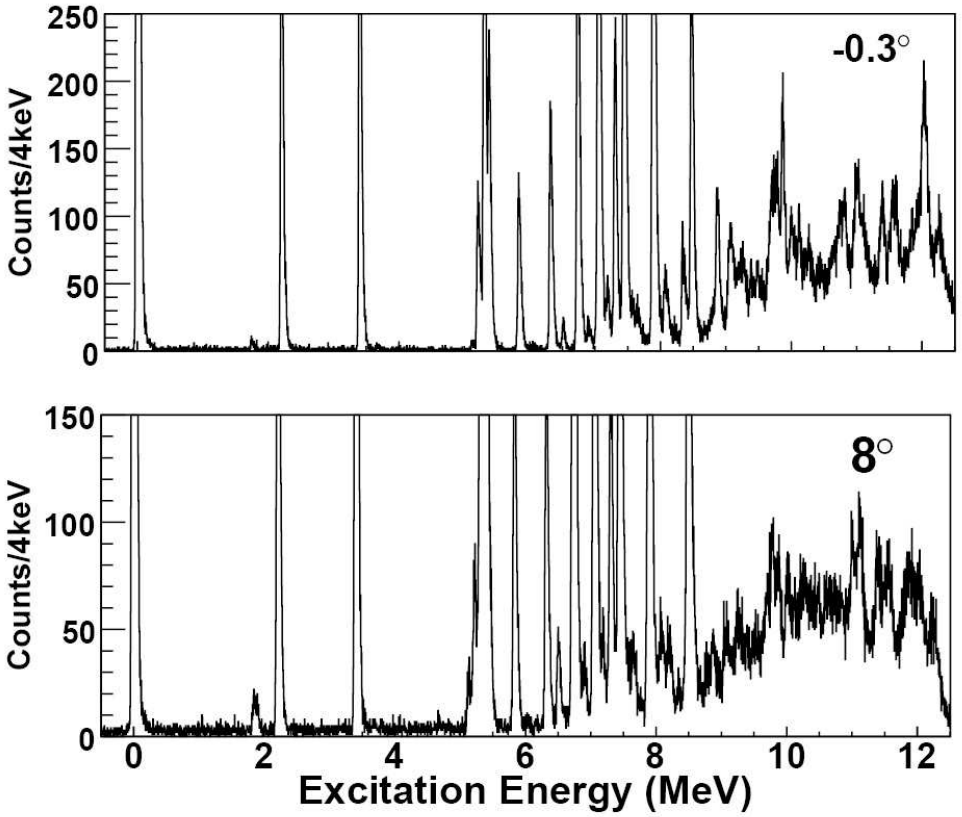

FIG. 1. A combined ^{32}S(p,t)^{30}S spectrum in the range from the g.s. up to 12.3 MeV excitation energy is shown for spectrometer angles of -0.3° and 8.0°.

III. THE $^{28}Si(^{3}He,n)$ EXPERIMENT

This experiment was carried out at the Nuclear Science Laboratory (NSL) at the University of Notre Dame. A 15 MeV ^{3}He pulsed beam with nanosecond-wide time resolution and 200 ns period was produced by the FN tandem accelerator at NSL and used to bombard a 90 μg/cm^2 thick self-supported natural Si target provided by Lebow Co. The schematic view of the experimental setup is shown in Fig. 2. The reaction products were measured by an array of 16 liquid-organic scintillation detectors which measured the neutrons from the reaction ^{28}Si(^{3}He,n) and a Low Energy Silicon-strip detector Array (LESA) [30, 31] which was used to measure the charged particle decays from the resonant levels in ^{30}S. The neutron detector array was placed 3.6 m away from the center of the reaction chamber covering an angular range from 11° to 39°. The beam stop was surrounded by plastic tanks filled with borated water in order to shield the detectors from background neutrons generated at the beam stop. The array of neutron detectors consisted of four hexagonal 12.7 cm (5″) thick detectors, five 17.78 cm × 2.54 cm (7″×1″) cylindrical detectors, and seven 12.7 cm × 5.08 cm (5″×2″) cylindrical detectors. The silicon detectors array LESA consisted of 4 identical 300 μm thick silicon-pad detectors, each of which has 4 strips of 1 cm wide × 4 cm long and a total area of 4×4 cm^2. The silicon detector array was installed inside the reaction chamber, 8 cm away from the target center covering an angular range from 90° to 150°. The neutron and silicon detectors were operated in coincidence mode to measure the decay products of the populated unbound states in ^{30}S.

A measurement with a pure carbon foil was also conducted in order to account for any background from carbon contamination of the target. The environmental background of the neutron ToF spectra was obtained from long runs without beam on target. The energy levels in ^{30}S were identified in the neutron detector array using Pulse Shape Discrimination (PSD) and ToF methods [32]. The PSD technique was performed with 4 - MPD4 Mesytec modules [33]. The neutron energy obtained from the ToF spectrum was used to identify the populated energy levels in ^{30}S.

A typical neutron ToF spectrum with the identification of different levels in ^{30}S up to E$_x$ = 10.0 MeV is shown in Fig. 3. The uncertainties in the ToF spectra are determined by the flight-path, the bunching uncertainty, the target

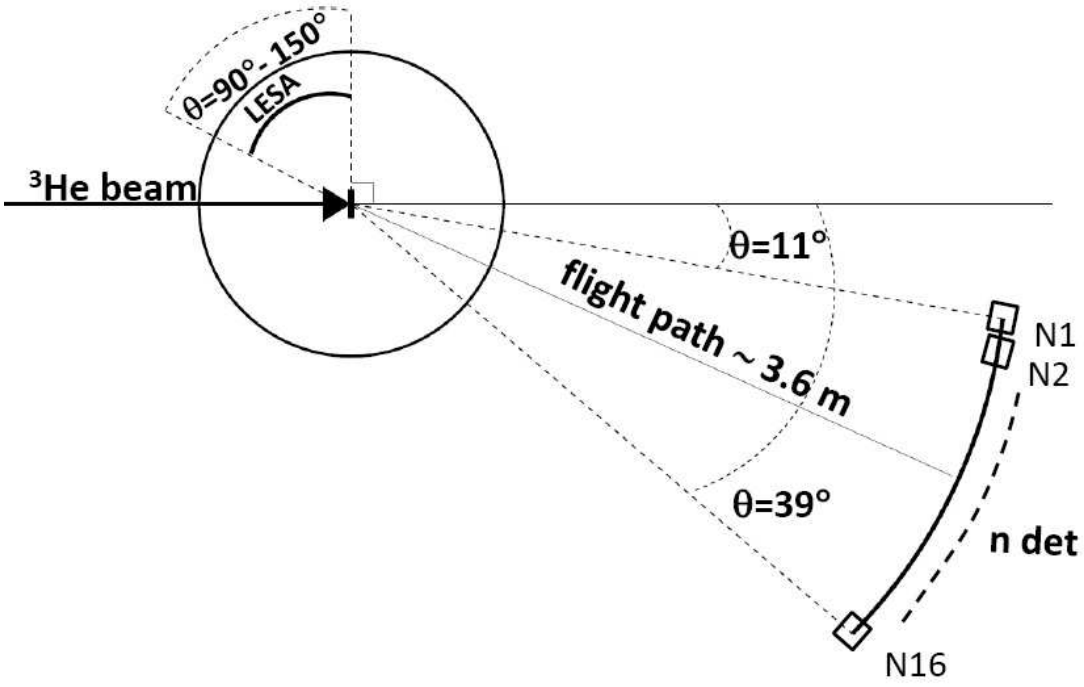

FIG. 2. Schematic view of the experimental setup of the ^{28}Si(^{3}He,n)^{30}S measurement. The neutron detectors were placed at 3.6 meters away from the center of the reaction chamber covering an angular range from 11° to 39°. The silicon detectors (LESA) were placed inside the reaction chamber covering an angular range from 90° to 150°.

thickness, the size of the neutron detectors and the statistical errors. The systematic and statistical errors are added linearly to account for the total uncertainty in energy. The uncertainties vary with the energy of the neutrons except for the bunching uncertainty that is a fixed value of 1.5 ns.

Levels above the proton threshold are expected to primarily decay by charged particle emission with the emitted protons or alphas for higher energy states being detected in the LESA silicon detector array. A complete kinematics reconstruction was performed to correlate the detected charged particles with the specific neutron group populating the unbound states. The higher-energy states in ^{30}S can decay into several proton channels populating excited states in ^{29}P. Primarily observed is the proton-decay to the ground-state of ^{29}P (p channel) and to the first seven excited states in ^{29}P at E$_x$ = 1.383 MeV, 1.954 MeV, 2.423 MeV, 3.106 MeV, 3.448 MeV, 4.080 MeV and 4.343 MeV (channels $p^{'}, p^{''}, p^{'''}, p^{iv}, p^{v}, p^{vi}$ and p^{vii} respectively). For the α-decay primarily transitions to the ground state of ^{26}Si were considered. After identifying the different decay channels, an event-by-event reconstruction for each energy level was made with the specific kinematic shifts for a chosen channel to add up all the sixteen strips of the silicon detectors. In the kinematic reconstruction of the proton spectra the resolution is dominated by the intrinsic resolution ($\sim$ 40 keV) of the silicon detectors and the comparable kinematics energy spread due to the width of the silicon strips. The energy spread and its effect on the resolution of the kinematics reconstruction is larger at forward angles and smaller at backward angles.

IV. RESULTS AND DISCUSSION

In the data analysis of the ^{32}S(p,t)^{30}S and the ^{28}Si(^{3}He,n)^{30}S experiments, a total of fifty-three states have been identified in ^{30}S. These states are sorted into three categories, five bound states below the proton threshold at 4.4 MeV, twenty-three proton-unbound states between 4.4 and 9.34 MeV, and twenty-five alpha-unbound states above 9.34 MeV. Of these fifty-three states, thirty-one levels have been identified for the first time. In the ^{32}S(p,t)^{30}S experiment, a total of forty-four states in ^{30}S have been identified, twenty-five levels for the first time. A triton spectrum showing the population of the different excited energy levels in ^{30}S is shown in Fig. 1. In comparison, in the ^{28}Si(^{3}He,n) measurement a total of thirty-one states in ^{30}S were identified, nine of them were not observed in

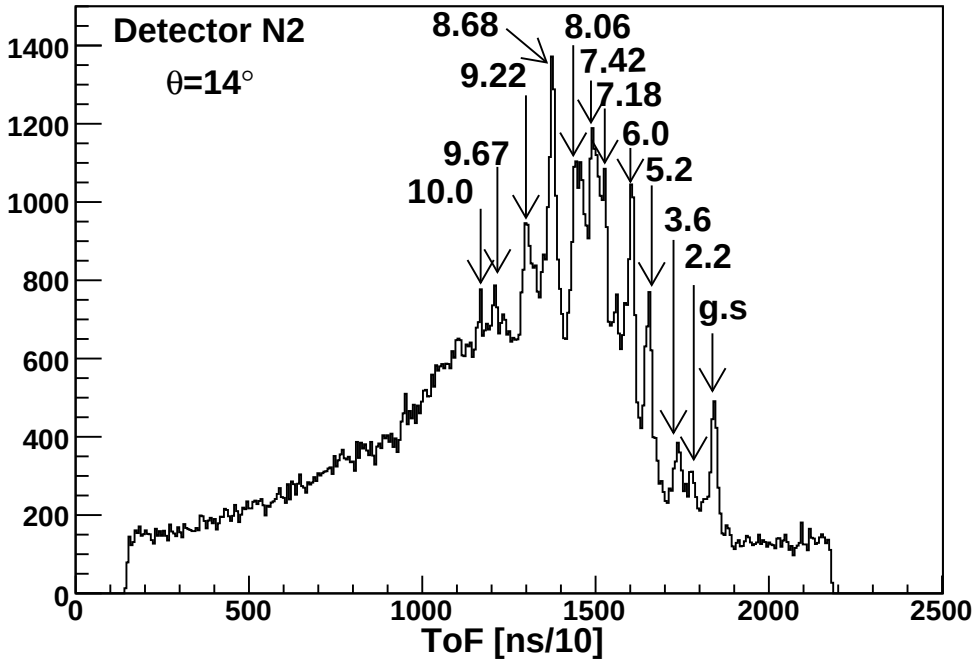

FIG. 3. Neutron ToF spectrum for neutron detector N2 at 14°. The identification of the different levels in ^{30}S up to E_x = 10 MeV is shown. Excitation energies in ^{30}S are given in MeV.

the ^{32}S(p,t)^{30}S experiment. For the analysis of the ^{28}Si(^{3}He,n) data, the neutron ToF spectra were gated with the signals from the LESA array corresponding to charged particle detection, in order to improve the identification of the proton-unbound states in ^{30}S. Typical neutron ToF spectra gated with the LESA signals are shown in Figs. 4, and 5.

In the following we discuss the various bound and unbound levels in ^{30}S based on the analysis of the ^{32}S(p,t)^{30}S and the ^{28}Si(^{3}He,n)^{30}S measurements described above. The spin-parity assignments are guided primarily by the level assignments in the mirror nucleus ^{30}Si. For proton-unbound states large shifts of level energies are expected and the assignments are based on two complementary methods associated with the two experiments. The ^{32}S(p,t)^{30}S reaction was measured for two spectrometer angle settings of -0.3° and 8°. The observed anisotropies in the yields of the various transitions were compared with DWBA predictions for the angular distributions calculated for orbital-momentum transfers of $\ell = 0$, 1, 2, 3, and 4. Higher spin assignments were not considered because previous experiments indicate that the (p,t) reaction populates preferably low-spin natural parity states [24, 25]. Further information is provided by the analysis of the proton-decay of the populated unbound states in ^{30}S observed in the ^{28}Si(^{3}He,n-p$_i$)^{30}S reaction. The strengths of the various proton-decay channels of the populated unbound states were measured using the ^{28}Si(^{3}He,n-p)^{29}P reaction and the energy spectra were reconstructed to extract the proton-branching ratios populating different excited states in ^{29}P. These strengths are associated with the orbital-momentum transfers, which provided further limitations for the spin assignments for the unbound states. The reconstructed energy spectra of the decaying particles in coincidence with neutrons are shown in Fig. 6 and 7 with different branching ratios shown in Tables III and V, respectively. The unlabeled peaks in these figures correspond to contamination from neighboring levels. The decay-branching ratios were measured for fifteen states in ^{30}S in the ^{28}Si(^{3}He,n-p)^{29}P experiment. Three of these states are above the α-decay threshold.

In the following section the results of the two experiments are discussed for each of the observed levels. Because there is complementary information from both experiments with respect to the specific configuration of the populated states we will first discuss the bound states in ^{30}S in the context of the previously available information. This will be followed by a discussion of the level parameters for proton-unbound states, which are of relevance for the determination of the ^{29}P(p,γ)^{30}S reaction. This will be followed by a discussion of the observed alpha-unbound states which are of relevance for the ^{26}Si(α,p)^{29}P reaction.

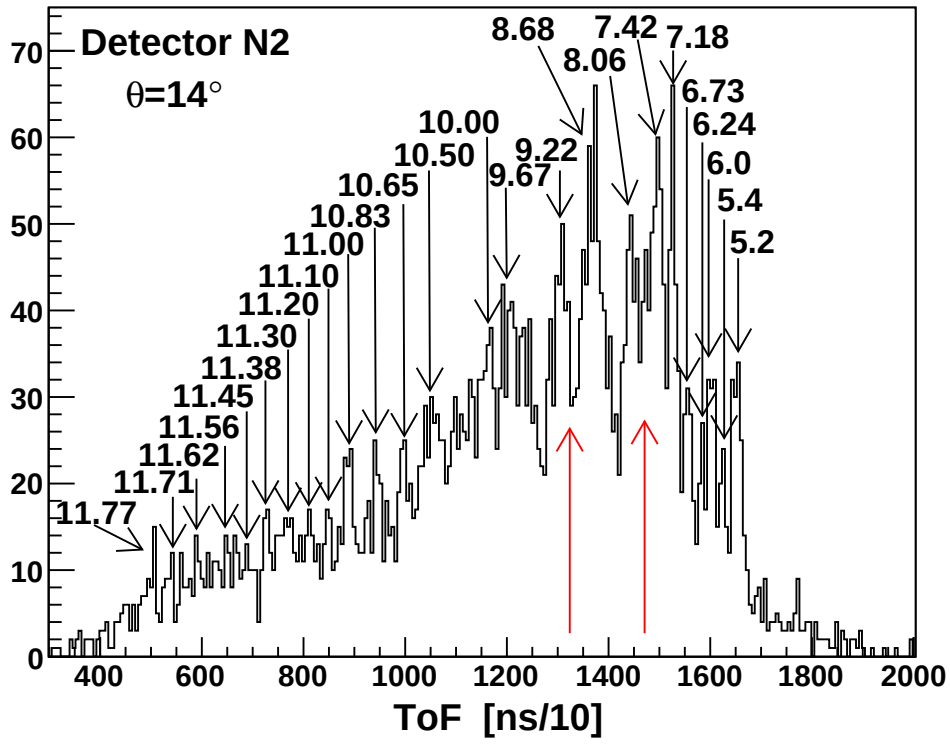

FIG. 4. LESA-gated neutron ToF spectrum for neutron detector N2 positioned at 14°. The ^{30}S levels marked by their excitation energies correspond to those charged particle decays that have been measured in the silicon detectors. The arrows indicate the position of possible background peaks associated with ^{14}O from ^{12}C target contamination. All excitation energies are given in MeV.

A. Bound states in ^{30}S below 4.40 MeV

The bound states in ^{30}S are well known and have been studied by ^{28}Si(^{3}He,n-γ)^{30}S coincidence measurements with high precision [19]. The excitation energies of the two excited 2^+ states are reported as 2.2107±0.0005 MeV and 3.4026±0.0005 MeV. A doublet was reported at 3.668±0.001 MeV and 3.676±0.003 MeV, corresponding to a doublet in ^{30}Si with 1^+ and 0^+ spin parity assignments. In the present experiment, the ^{32}Si(p,t) analysis gives excitation energies for the two lowest-lying 2^+ states at E_x = 2.2085±0.0024 MeV, and 3.4058±0.0015 MeV, while the doublet was recorded as an unresolved doublet at 3.6773±0.0071 MeV. The ^{28}Si(^{3}He,n)^{30}S ToF measurements determined excitation energies of E_x = 2.200±0.210 MeV and 3.600±0.260 MeV, with the second 2^+ state and the doublet remaining unresolved due to the limited resolution associated with the short flight path. These results are in good agreement with recent high resolution ^{32}S(p,t)^{30}S studies [10, 22] except for a small discrepancy in the energy of the second 2^+ state. This agreement demonstrates that the level structure of ^{30}S below the proton threshold is well understood and the level energies serve as additional calibration points for the energy determination of higher-excited states. A summary of the results on the excitation energies of the bound states in ^{30}S in the present ^{32}S(p,t)^{30}S and ^{28}Si(^{3}He,n)^{30}S experiments and their comparison with the results of previous works is shown in Table I.

B. Proton-unbound states in ^{30}S below 9.34 MeV

The analysis of the ^{32}S(p,t) and ^{28}Si(^{3}He,n) transitions to proton-unbound states in ^{30}S agrees well with previous studies. The previous studies were limited to excitation energies below 8 MeV, while the present studies cover considerably higher energies as well. The ^{32}S(p,t)^{30}S spectra indicate 20 proton-unbound levels in this excitation range and the excitation energies could be determined with 10 to 50 keV accuracy, depending on the strength of the various transitions. In comparison only 12 states were observed in ^{28}Si(^{3}He,n)^{30}S. Despite the rather limited resolution in the ToF measurements, the excitation energy could be reconstructed with improved accuracy by analyzing the proton

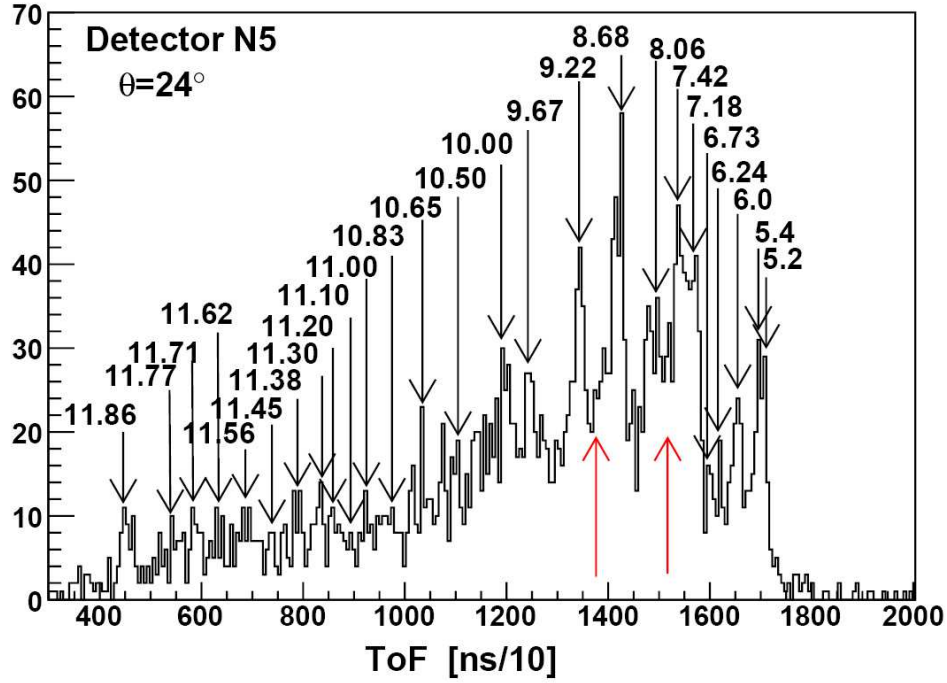

FIG. 5. LESA-gated neutron ToF spectrum for neutron detector N5 positioned at 24°. Several unbound levels in ^{30}S are identified with decays recorded by the silicon detectors. The arrows indicate the position of background peaks of ^{14}O from possible ^{12}C target contamination. All excitation energies are given in MeV.

TABLE I. Energy levels below the charged-particle threshold in ^{30}S measured in the present experiments and comparison with previous results. Excitation energies are given in MeV.

This work		Bardayan *et al.* [10]		Paddock [17]	Kuhlmann *et al.* [19]		Caraça *et al.* [18]	Setoodehnia *et al.* [22]
^{32}S(p,t)^{30}S	^{28}Si(^{3}He,n)^{30}S	^{32}S(p,t)^{30}S		^{32}S(p,t)^{30}S	^{28}Si(^{3}He,nγ)^{30}S		^{28}Si(^{3}He,nγ)^{30}S	^{32}S(p,t)^{30}S
			J^π			J^π		
g.s.	g.s.	0.000000(4)	0^+	g.s.				
2.2085(22)	2.20(21)	2.2107	2^+	2.239(18)	2.2107(5)	2	2.2099(11)	2.2106
3.4058(12)		3.4026	2^+	3.438(14)	3.4026(5)	1, 2	3.4022(13)	3.4026
	3.60(26)				3.6675(10)		3.6642(13)	
3.6773(70)		3.680(6)	(1^+)	3.707(25)	3.676(3)	1		3.680 (4)

decays of the various observed levels. A summary of the observed excitation energies of the proton-unbound states in ^{30}S up to the alpha-threshold is shown in Table II and compared to the results of previous studies.

The strengths of the various proton-decay channels of the populated unbound states were measured using the ^{28}Si(^{3}He,n-p)^{29}P reaction and the energy spectra were reconstructed to extract the proton-branching ratios populating different excited states in ^{29}P. The reconstructed energy spectra of the decay particles in coincidence with neutrons are shown in Fig. 6 with their corresponding branching ratios listed in Table III. A summary of the states between the proton-decay threshold (E_x = 4.399 MeV) and the α-decay threshold (E_x = 9.343 MeV) in ^{30}S observed in the ^{28}Si(^{3}He,n-p)^{29}P experiment is also shown in Table III. For these twelve states, information on the excitation energy as well as the branching ratio of the potential resonant levels of ^{30}S is given. These states are relevant in the calculation of the astrophysically important ^{29}P(p,γ)^{30}S reaction rate. In the following section we discuss in more detail the experimental observations and the conclusions drawn with respect to the energy and spin-parity assignments of the observed levels.

The first state above the proton threshold at E_x = 4.6825±0.0058 MeV is only weakly observed in the measured ^{32}S(p,t) spectra but corresponds most likely to the previously observed state at 4.704±0.005 MeV [10] and 4.693±0.005 MeV [22]. This level has been identified as the previously predicted low-energy 3^+ state in ^{30}S [10]. The states observed

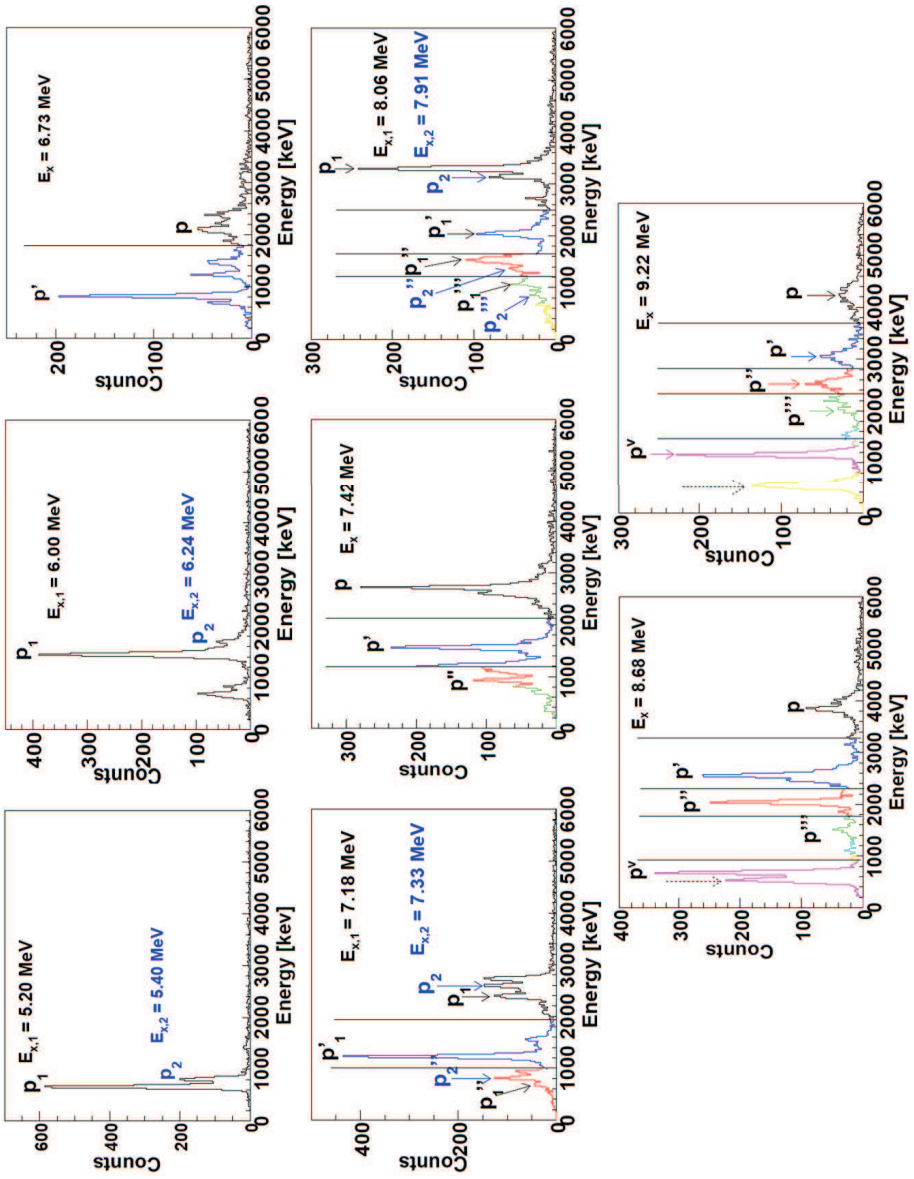

FIG. 6. (Color online) Event-by-event reconstructed spectra for different energy levels in ^{30}S between the proton-decay threshold and α-decay threshold measured in the present ^{28}Si(^{3}He,n-p) experiment. The different colors separated by vertical lines correspond to different kinematics used to reconstruct different portions of the spectra. Notice that several panels contain peaks corresponding to two different energies as indicated by subscripts, e.g. p_1 belonging to $E_{x,1}$. This is due to the fact that those peaks are not well resolved in the neutron detectors (ToF spectra) but they are well separated in the LESA silicon detectors where all the decays are identified and followed. Such is the case for the levels at E_x = 5.20 MeV and E_x = 5.40 MeV, E_x = 6.00 MeV and E_x = 6.24 MeV, E_x = 7.18 MeV and E_x = 7.33 MeV as well as E_x = 8.06 MeV and E_x = 7.91 MeV. In several spectra, contamination from neighboring peaks is observed (unlabeled peaks). The low energy peak present in the spectra corresponding to E_x = 8.68 MeV and E_x = 9.22 MeV marked by the dashed arrow, arises due to the presence of carbon contamination in the target. The branching ratios are listed in Table III.

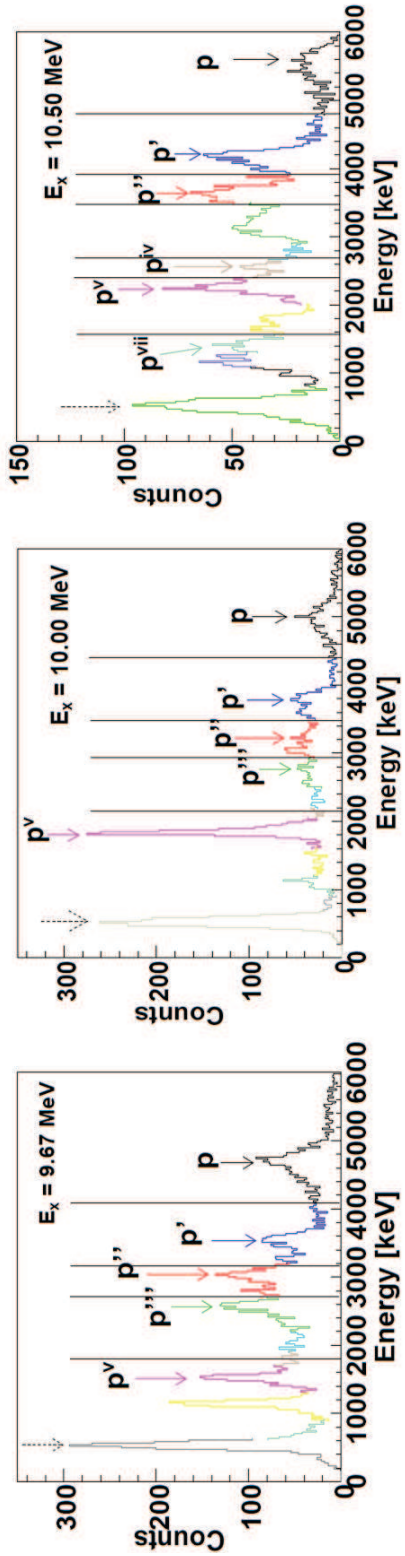

FIG. 7. (Color online) Event-by-event reconstructed spectra for different energy levels in ^{30}S above the α-decay threshold measured in the present ^{28}Si(^{3}He,n-p) experiment. The different colors separated by vertical lines correspond to different kinematics used to reconstruct different portions of the spectra. The low energy peak present in the spectra and marked by the dashed arrow, arises due to the presence of carbon contamination in the target. In some cases, contamination from neighboring energy levels is observed (unlabeled peaks). The branching ratios are listed in Table V.

TABLE II. Energy levels between the proton-decay threshold and α-decay threshold in ^{30}S measured in the present experiments and comparison with previous results. Excitation energies are given in MeV.

This work			Fynbo *et al.* [21]	Yokota *et al.* [20]		Bardayan *et al.* [10]		Paddock [17]	Setoodehnia *et al.* [22]
^{32}S(p,t)^{30}S	^{28}Si(^{3}He,np)^{30}S	J^π	^{31}Ar(β^+)(p)^{30}S	^{28}Si(^{3}He,np)^{30}S	J^π	^{32}S(p,t)^{30}S	J^π	^{32}S(p,t)^{30}S	^{32}S(p,t)^{30}S
4.6825(57)						4.704(5)			4.693(5)
									4.814(3)
5.1300(18)		4^+		5.145		5.168(6)	$4^+ + 0^+$	5.207(22)	5.136
5.2178(28)	5.200(44)	0^+	5.2174(7)						5.226(3)
5.3121(20)		3^-		5.288	3^-			5.306(25)	5.318(4)
5.3820(7)	5.400(43)	2^+	5.389(2)	5.425	(1,2)	5.383(8)	$(3^-, 2^+)$	5.426(25)	5.396(4)
5.8355(13)		4^+	5.842(4)	5.912	(3,4)	5.843(5)	(1^-)	5.897(27)	
			(5.945(3))						
	6.000(41)		6.064(3)	6.117	1^-	6.071(11)		(6.108(29))	
	6.240(42)		6.202(3)	6.233				(6.223(30))	
			6.2801(12)						
6.3259(7)		0^+	6.3386(14)	6.393	0^+	6.341(5)		6.415(40)	
6.5121(33)		(1^-)	6.541(4)	6.584	(2,3)	6.532(13)			
			(6.643(3))						
6.7375(7)	6.730(44)	2^+	6.762(4)	6.810		6.766(10)	2^+	6.861(40)	
			6.855(4)	6.838	$\geq$4				
6.9015(23)		(1^-)	6.927(4)	6.919	(3,4)				
7.0589(25)		0^+	7.078(7)	7.133	(1,2)	7.074(9)		7.185(35)	
			7.123(10)						
7.1949(18)	7.180(41)	3^-	(7.237(5))	7.294	$\geq$3				
			7.295(14)						
7.3106(7)	7.330(44)	(2^+)	7.352(8)	7.338	(1,2)				
7.4465(12)	7.420(45)	(4^+)	7.485(4)	7.475					
			7.598(4)					7.570(45)	
			7.693(4)						
7.8990(8)	7.910(49)		7.924(5)						
8.0828(23)	8.060(51)								
8.4823(15)									
	8.680(44)								
8.8750(82)									
9.0806(45)									
9.2763(42)	9.220(41)								

at 5.1300±0.0020 MeV and 5.2178±0.0029 MeV correspond to previously reported states [17, 19–22]. Bardayan *et al.* [10] quote only one level for this excitation range. Based on previous arguments about the mirror structure in the ^{30}S - ^{30}Si system [10, 15, 19, 35], we adopt a spin-parity of 4^+ for the 5.130 MeV state and spin-parity of 0^+ for the state at 5.218 MeV. With these assignments, we assume the 5.130 MeV and 5.218 MeV states to be the mirrors of the 5.280 MeV and 5.372 MeV states in ^{30}Si. The doublet could not be resolved in our ^{28}Si(^{3}He,n) measurement. A proton-decay in the range of 98-100 % was observed to the $1/2^+$ ground state of ^{29}P, which is most likely associated with the the decay of the 0^+ state at 5.218 MeV.

The states observed at 5.3121±0.0022 MeV, 5.3820±0.0011 MeV and 5.8355±0.0016 MeV in the ^{32}S(p,t) spectra are believed to be the same as those observed previously [20] at 5.288 MeV, 5.425 MeV and 5.912 MeV, respectively and more recently at 5.318 MeV and 5.396 MeV [22]. These states are assumed to be the mirrors of the levels in ^{30}Si found at 5.487 MeV, 5.614 MeV and 5.950 MeV, respectively. Based on this mirror assignment, we adopt 3^- for the 5.312 MeV state, 2^+ for the level at 5.382 MeV and 4^+ for the state at 5.836 MeV. The 2^+ level at 5.382 MeV is observed to decay 96-100 % to the ground state of ^{29}P. No significant proton-decay is observed for a state at 5.836 MeV, which indicates that the proton-decay is suppressed by a high orbital-momentum barrier supporting the 4^+

TABLE III. Summary of results obtained from the energy levels in ^{30}S between the proton-decay threshold and the α-decay threshold in the present ^{28}Si(^{3}He,n-p) experiment. Excitation energies, branching ratios (BR) and partial-widths are provided.

^{30}S E_x (MeV)	Branching Ratios (BR)	Partial Widths
5.200±0.044	BR_p=1.00±0.02	
5.400±0.043	BR_p=1.00±0.04	
6.000±0.041	BR_p=1.00±0.02	
6.240±0.042	BR_p=1.00±0.06	
6.730±0.044	BR_p=0.14±0.04	
	$BR_{p'}$=0.86±0.16	$\frac{\Gamma_{p'}}{\Gamma_p}$=6.14
7.180±0.041	BR_p=0.28±0.05	
	$BR_{p'}$=0.64±0.07	$\frac{\Gamma_{p'}}{\Gamma_p}$=2.29
	$BR_{p''}$=0.08±0.02	$\frac{\Gamma_{p''}}{\Gamma_p}$=0.29
7.330±0.044	BR_p=0.63±0.05	
	$BR_{p''}$=0.37±0.09	$\frac{\Gamma_{p''}}{\Gamma_p}$=0.59
7.420±0.045	BR_p=0.37±0.08	
	$BR_{p'}$=0.43±0.06	$\frac{\Gamma_{p'}}{\Gamma_p}$=1.16
	$BR_{p''}$=0.20±0.04	$\frac{\Gamma_{p''}}{\Gamma_p}$=0.54
7.910±0.049	BR_p=0.58±0.10	
	$BR_{p''}$=0.38±0.25	$\frac{\Gamma_{p''}}{\Gamma_p}$=0.65
	$BR_{p'''}$=0.04±0.02	$\frac{\Gamma_{p'''}}{\Gamma_p}$=0.07
8.060±0.051	BR_p=0.48±0.05	
	$BR_{p'}$=0.17±0.07	$\frac{\Gamma_{p'}}{\Gamma_p}$0.35
	$BR_{p''}$=0.25±0.10	$\frac{\Gamma_{p''}}{\Gamma_p}$=0.52
	$BR_{p'''}$=0.10±0.08	$\frac{\Gamma_{p'''}}{\Gamma_p}$=0.21
8.680±0.044	BR_p=0.10±0.02	
	$BR_{p'}$=0.25±0.08	$\frac{\Gamma_{p'}}{\Gamma_p}$2.5
	$BR_{p''}$=0.24±0.08	$\frac{\Gamma_{p''}}{\Gamma_p}$=2.4
	$BR_{p'''}$=0.03±0.01	$\frac{\Gamma_{p'''}}{\Gamma_p}$=0.3
	BR_{p^v}=0.38±0.10	$\frac{\Gamma_{p^v}}{\Gamma_p}$=3.8
9.220±0.041	BR_p=0.10±0.03	
	$BR_{p'}$=0.19±0.06	$\frac{\Gamma_{p'}}{\Gamma_p}$=1.9
	$BR_{p''}$=0.23±0.05	$\frac{\Gamma_{p''}}{\Gamma_p}$=2.3
	$BR_{p'''}$=0.06±0.02	$\frac{\Gamma_{p'''}}{\Gamma_p}$=0.6
	BR_{p^v}=0.42±0.08	$\frac{\Gamma_{p^v}}{\Gamma_p}$=4.2

assignment in agreement with previous suggestions [20].

Previously observed levels in the excitation range between 6.0 and 6.3 MeV were not observed in the ^{32}S(p,t) spectra at the two angle positions of the spectrometer. However the states are strongly populated by the ^{28}Si(^{3}He,n) reaction [20] and a 100 % decay into the proton channel was observed. This observation is confirmed in the present work and the corresponding excitation energies have been determined to be 6.000±0.041 MeV and 6.240±0.042 MeV.

The state observed at 6.3259±0.0011 MeV in the ^{32}S(p,t) spectra corresponds to the level at 6.3386 MeV, which was previously identified in the β-delayed proton-decay of ^{31}Ar [21] and at 6.393 MeV in the ^{28}Si(^{3}He,n-p)^{29}P analysis by Yokota et al. [20]. Based on these data a $J^\pi = 0^+$ assignment was suggested. This agrees well with the present results where a large ^{32}S(p,t) cross section anisotropy between -0.3° and 8° also indicates a 0^+ assignment. This level, however could not be clearly identified in the present ^{28}Si(^{3}He,n-p)^{29}P experiment due to the limited statistics in the proton spectra. Based on the 0^+ spin-parity assignment, we assume this state to be the mirror of the 6.642 MeV state in ^{30}Si.

The state observed at 6.5121±0.0034 MeV in the ^{32}S(p,t) experiment corresponds to the level at 6.541 MeV which was observed in the β-delayed proton-decay of ^{31}Ar [21] and in the ^{28}Si(^{3}He,n-p)^{29}P experiment by Yokota et al.

[20]. Again, the statistics in the present ^{28}Si(^{3}He,n-p)^{29}P experiment was not sufficient for a clear identification and energy assignment of this level. Since this level is clearly visible in the (p,t) reaction, which shows a preference for natural parity states, we tentatively assume this state to be the mirror of the 6.744 MeV 1^- level in ^{30}Si.

The state observed at 6.737 MeV in the ^{32}S(p,t) experiment is thought to be identical with the state observed at 6.762 MeV in the β-delayed proton-decay of ^{31}Ar [21]. The spin assignment is adopted to be 2^+ [10] assuming it to be the mirror of the level at 6.915 MeV in ^{30}Si. The proton-decay spectrum has been measured in the present ^{28}Si(^{3}He,n-p)^{29}P study and suggests a 14±4 % branch to the $1/2^+$ ground-state in ^{29}P and a branch in the range of 70-100 % to the $3/2^+$ first excited state at 1.384 MeV. This ratio reflects the difference in orbital-momentum barrier for a d-wave decay to the ground-state versus an s-wave decay to the first-excited state, which supports the above 2^+ spin assignment.

The state observed at 6.901 MeV in the ^{32}S(p,t) experiment has not been reported before. However, it could correspond to the previously reported levels at 6.927 MeV [21] or 6.919 MeV [20]. This level was not observed in the present ^{28}Si(^{3}He,n-p)^{29}P experiment due to limited statistics. Since the state is clearly populated in the (p,t) reaction which preferably populates natural parity states and due to the very similar pattern observed in its population with the level observed at 6.512 MeV, we tentatively assign the spin-parity (1^-).

The state at 7.059 MeV in the present ^{32}S(p,t) measurement was also observed by Bardayan *et al.* at 7.074 MeV [10] as the state of highest excitation energy covered by that study. This energy agrees well with the results from the β-delayed proton-decay of ^{31}Ar which assigned a value of 7.078 MeV [21]. This state exhibits a large ^{32}S(p,t) cross section ratio between -0.3° and 8° suggesting a spin-parity assignment of 0^+. The proton decay of this state could not be observed in the present ^{28}Si(^{3}He,n-p)^{29}P experiment.

The state observed at 7.1949±0.0020 MeV is thought to be identical to the tentatively identified level at (7.237) MeV [21] or 7.294 MeV [20]. It was also observed in the present ^{28}Si(^{3}He,n-p)^{29}P study yielding a proton-decay branching of 28±5 % to the ground-state, 64±7 % to the $3/2^+$ first-excited state and 8±2 % to the $5/2^+$ second-excited state at 1.954 MeV. While previous results suggest a spin of 3 or greater the observed proton decay branching ratios match best with a f-wave transition to the ground state and a p-wave transition to the two first excited states in ^{29}P; we therefore suggest a 3^- spin-parity assignment for this level.

Two pronounced levels were also observed at energies of 7.3106 MeV and 7.4465 MeV in the ^{32}S(p,t) spectra, which correspond to a cluster of states observed in the β-delayed proton-decay of ^{31}Ar [21]. These states are also observed in the ^{28}Si(^{3}He,n-p)^{29}P proton spectra; the first level shows a proton-decay branching of 63±5 % to the ground-state and 37±9 % to the second-excited state in ^{29}P. The transition to the first-excited state is rather weak and could not be resolved due to contaminations from the decay of neighboring levels. This resembles a rather odd decay pattern most likely coming from an unresolved doublet with the lower spin component decaying preferably to the $1/2^+$ ground-state in ^{29}P while the level with the higher-spin value decays to the $5/2^+$ second-excited state in ^{29}P. The mirror states in ^{30}Si could be the 2^+ and the 4^+ states at 7.623 MeV and 7.810 MeV, respectively. The 7.446 MeV state was identified in the proton spectrum with an energy of 7.42 MeV and a 37±8 % decay to the ground-state, 43±6 % to the first-excited state and 20±4 % to the second-excited state in ^{29}P. Again, this probably reflects the decay pattern of an unresolved doublet configuration corresponding to a cluster of 2^+, and 4^+ states near 8.0 MeV in the mirror nucleus ^{30}Si.

The ^{32}S(p,t) spectra also indicate a strong transition to a state at 7.899 MeV with a second weakly populated level at 8.08 MeV. The proton decay of both configurations has been observed in the ^{28}Si(^{3}He,n-p)^{29}P experiment which suggests excitation energies of 7.91 MeV and 8.06 MeV. The 7.91 MeV level decays primarily with 58±10 % to the ground-state and to 38±25 % to the second-excited state with a third weak transition of 4±2 % to the $3/2^+$ third-excited state at 2.423 MeV in ^{29}P. A similar complex decay pattern is observed for the level configuration near 8.06 MeV with a 48±5% decay to the ground-state, a 17±7 % decay to the first-excited state, 25±10 % branch to the second-excited state and finally a weak 10±8% decay to the third-excited state. Again, orbital-momentum transfer arguments exclude that this can reflect the decay pattern of a single level and is probably associated to the decay of a number of unresolved states in the excitation range near 8.0 MeV in ^{30}S. Indeed, the level structure in the corresponding excitation energy range in the mirror nucleus ^{30}Si is characterized by a cluster of 1^-, 2^+, and 5^- states near 8.2 MeV and a second group of 3^- and 4^+ states near 8.5 MeV, which could explain a complex proton-decay pattern through a mixture of orbital-momenta as observed.

Further level configurations near the alpha threshold were discovered in the ^{32}S(p,t) spectra at 8.482 MeV and 8.875 MeV. Corresponding to that energy range the ^{28}Si(^{3}He,n-p)^{29}P proton spectra indicate the decay of a 8.68 MeV configuration to the ground-state, the first three excited states, as well as the $7/2^+$ fifth-excited state in ^{29}P. A similar decay pattern is observed for the configuration at 9.22 MeV, which was also identified in the ^{32}S(p,t) spectrum with levels at 9.081 and 9.276 MeV excitation energy. Again, the mirror nucleus shows in the corresponding excitation range a rather high level density, which corresponds to a large number of states in ^{30}S reflected in the collective proton-decay of unresolved states populated in the ^{28}Si(^{3}He,n-p) transfer reaction.

TABLE IV. Energy levels above the α-decay threshold at E_x = 9.343 MeV in ^{30}S measured in the present experiments. Excitation energies are given in MeV.

This work		
^{32}S(p,t)^{30}S	^{28}Si(^{3}He,np)^{30}S	J^π
9.3914(65)		$(0^+, 1^-, 2^+)$
9.4860(74)		
9.7012(56)	9.670(41)	$(0^+, 1^-, 2^+)$
9.7851(44)		
9.8742(91)		$(0^+, 1^-, 2^+)$
10.0088(208)	10.000(41)	
10.0705(55)		
10.1226(15)		
10.2747(19)		
10.4431(46)	10.500(43)	
	10.650(43)	
10.7551(30)		
10.8149(28)	10.830(40)	
11.0154(8)	11.000(35)	
	11.100(35)	
	11.200(32)	
	11.300(32)	
11.3997(22)	11.380(26)	
11.4904(33)	11.450(24)	
11.5462(20)	11.560(23)	
11.6091(25)	11.620(26)	
11.6817(40)	11.710(20)	
	11.770(19)	
11.8523(37)	11.860(20)	
12.0392(23)		

C. Alpha-unbound states in ^{30}S above 9.343 MeV

A number of alpha-unbound states were observed for the first time in the present experiments. Similar to the case of proton-unbound states, some levels were observed in both experiments while some were detected in only one experiment and not the other. The excitation energies were determined for all observed levels and are listed in Table IV.

For the twenty states observed in the ^{32}S(p,t)^{30}S experiment in this energy region, the states measured at 9.3914±0.0065, 9.7012±0.0056 and 9.8742±0.0091 MeV have cross-section ratios of 3 to 5 between the angles of -0.3° and 8°. This suggests an angular momentum ≤ 2 and spin-parities of 0^+, 1^- or 2^+.

In the ^{28}Si(^{3}He,n-p)^{29}P experiment a total of sixteen states above the α-decay threshold were measured. Branching ratios were extracted for three levels located at E_x = 9.670±0.041 MeV, E_x = 10.000±0.041 MeV and E_x = 10.500±0.043 MeV. The results for the branching ratios measured for these levels are shown in Table V. For the remaining thirteen states the branching ratios were not measured because the energy of the proton decaying to the ground state of ^{29}P is outside the range of the silicon detectors (6 MeV).

In the present experiments, no spin assignment could be made for the observed alpha-unbound states at energies above 10 MeV. The resonance states above the α-decay threshold would be relevant in the calculation of the astrophysically important ^{26}Si(α,p)^{29}P reaction rate.

D. The level structure of ^{30}S

The tentative spin assignments were made using all available experimental information of this work. Due to the high centrifugal barriers we assume that the spins of the states are generally between 0 and 4. From the (p,t) data,

TABLE V. Summary of states observed in ^{30}S above the α-decay threshold at E$_x$ =9.343 MeV measured in the present ^{28}Si(^{3}He,n-p) experiment for which the branching ratios were measured. Excitation energies, branching ratios (BR) and partial-widths are provided.

^{30}S E$_x$ (MeV)	Branching Ratio (BR)	Partial Widths
9.670±0.041	BR$_p$=0.13±0.03	
	BR$_{p'}$=0.17±0.06	$\frac{\Gamma_{p'}}{\Gamma_p}$=1.31
	BR$_{p''}$=0.23±0.06	$\frac{\Gamma_{p''}}{\Gamma_p}$=1.77
	BR$_{p'''}$=0.20±0.07	$\frac{\Gamma_{p'''}}{\Gamma_p}$=7.54
	BR$_{p^v}$=0.27±0.05	$\frac{\Gamma_{p^v}}{\Gamma_p}$=2.08
10.000±0.041	BR$_p$=0.11±0.05	
	BR$_{p'}$=0.12±0.06	$\frac{\Gamma_{p'}}{\Gamma_p}$=1.01
	BR$_{p''}$=0.11±0.06	$\frac{\Gamma_{p''}}{\Gamma_p}$=1.0
	BR$_{p'''}$=0.10±0.07	$\frac{\Gamma_{p'''}}{\Gamma_p}$=0.91
	BR$_{p^v}$=0.56±0.10	$\frac{\Gamma_{p^v}}{\Gamma_p}$=5.09
10.500±0.043	BR$_p$=0.04±0.01	
	BR$_{p'}$=0.26±0.08	$\frac{\Gamma_{p'}}{\Gamma_p}$=6.5
	BR$_{p''}$=0.30±0.09	$\frac{\Gamma_{p''}}{\Gamma_p}$=7.5
	BR$_{p^{iv}}$=0.08±0.03	$\frac{\Gamma_{p^{iv}}}{\Gamma_p}$=2.0
	BR$_{p^v}$=0.19±0.06	$\frac{\Gamma_{p^v}}{\Gamma_p}$=4.75
	BR$_{p^{vii}}$=0.13±0.04	$\frac{\Gamma_{p^{vii}}}{\Gamma_p}$=3.25

the ratio of the cross-sections at -0.3° and 8° are generally large for the population of 0^+ and 2^+ states (this ratio is 2.7 for the case of the 0^+ ground state of ^{30}S and 1.5 for the 2^+ first excited state). Therefore, the ratio of the cross-sections taken at these different angles can be used to constrain the set of possible spins. Typical ratios for specific spin values have been taken from levels with previously confirmed spin assignments. The calculated proton widths are used to discard spin assignments that imply proton widths larger than the experimentally measured ones. The experimentally measured widths of the states as well as the proton-partial widths were also used to constrain the spins of the levels in ^{30}S by comparing them with the calculated values.

The calculation of the proton-partial widths Γ_p was done using the expression:

$$\Gamma_p = C^2 S \Gamma_{sp} \tag{1}$$

where C^2S is the spectroscopic factor and Γ_{sp} denotes the partial width of a single-particle resonance located at the same energy as the resonance of interest [34]. The partial widths Γ_{sp} were computed using the code DWUCK4 [36]. In the determination of the partial widths Γ_{sp} using DWUCK4 it is necessary to specify the quantum numbers N (number of nodes of the wave function) and the angular momentum ℓ for the resonance state. Using shell model calculations it is possible to determine which orbital may be populated by the valence protons given the number of protons in the core and therefore, determining n and ℓ for that state where $N = n$ - *1*. In the calculation of the spin and angular momentum transfer of the ^{29}P+p system, it was assumed that they couple to the state of minimum spin and angular momentum available. When possible, the spectroscopic factors were assumed from the corresponding mirror states. In absence of spectroscopic factor information, values of 0.1 for C^2S were assumed for states below the α-decay threshold and 0.01 for states above it. The widths of the states were extracted from the experimental data and compared with the calculated values. The resolution of the ^{32}S(p,t) experiment is better than the ^{28}Si(^{3}He,n) experiment, so we used the (p,t) set of data to measure the widths of the states whenever the states in (^{3}He,n) data matched the energy of states in the (p,t) data. The measured intrinsic width of the ^{32}S(p,t) data is $\Gamma_{int} = 45 \pm 5$ keV, while the measured intrinsic width of the ^{28}Si(^{3}He,n) is $\Gamma_{int} = 70 \pm 10$ keV. The total measured widths of the states were extracted using the relation $\Gamma = \sqrt{\Gamma^2_{meas} - \Gamma^2_{int}}$. After constraining the spin assignments of the resonant levels, we calculated the corresponding γ- or α-widths to be used in the calculations of the (p,γ) or (α,p) reaction rates. The γ-widths needed for the (p,γ) reaction rates were calculated based on the lifetimes of the mirror states, when possible. In absence of experimental information, the γ-widths were calculated using "average γ transition strengths" [5]. Only the most probable transitions (E1, M1 and E2) were used in the calculations of the gamma-widths according to the expressions:

$$\Gamma_\gamma(M1) = 10^{-1.25} 2.1 \times 10^{-2} E_\gamma^3 \tag{2}$$

$$\Gamma_\gamma(E1) = 10^{-3.5} 6.8 \times 10^{-2} A^{2/3} E_\gamma^3 \tag{3}$$

$$\Gamma_\gamma(E2) = 10^{0.5} 4.9 \times 10^{-8} A^{4/3} E_\gamma^5 \tag{4}$$

where, Γ_γ are the γ-widths (eV), A is the mass of the nucleus (amu) and E_γ are the transition energies (MeV).

In the present experiments, states above the α-decay threshold in ^{30}S are measured for the first time. In order to provide tentative spin assignments for these energy levels, we compared the experimental information from the branching ratios of the ^{28}Si(^{3}He,n) data to the calculations for the proton-partial and total widths to constrain the tentative spin assignments. In the case where no experimental branching ratios were obtained ($E_x \geq 10.5$ MeV) only the total proton-widths were used for the tentative spin assignments. For the energy levels above the α-decay threshold and after a tentative spin assignment, α-widths were calculated using Eq. 1. The α-widths were calculated using DWUCK4 code [36]. The calculation of the quantum numbers needed to input in DWUCK4 is slightly more difficult than for the proton width calculations. In this case, a ^{26}Si+α system is considered. The quantum numbers N, number of nodes of the wave function, and $L = \ell$ relative angular momentum of the α particle are needed. As both the core (^{26}Si) and the α-cluster have total spin equal to 0 in their ground states, the angular momentum L of the α particle must be equal to the spin of the resonant state in ^{30}S. The determination of the number of nodes of the wave function was done with the prescription given by Mohr using the Wildermuth condition [37]:

$$Q = 2N + L = \sum_{i=1}^{4} q_i \tag{5}$$

where Q is the number of oscillator quanta, N is the number of nodes, L is the relative angular momentum of the α particle and q_i are the corresponding quantum numbers of the nucleons in the α-cluster. For the present case, $Q = \sum q_i = 8$ or 9 for states with even or odd spin, respectively. Knowing the values of Q and L, the value of N can be determined and the corresponding α-width calculated.

For the energy levels above $E_x = 10.5$ MeV, the branching ratios could not be measured because the energy in the silicon detectors of the corresponding proton-decay to the ground state of ^{29}P is higher than 6 MeV, which is outside of our energy range. The proton-widths and partial widths were calculated considering that the proton-decay would populate excited states in ^{29}P up to the fifth excited state, as it was observed in most of the cases for lower-lying levels. In this way the total widths were calculated and compared with the measured values. This condition just excluded one, two and in few cases, three possible spins, for example, in most cases spin 2 is excluded due to the very large proton-width resulting from the calculations.

After all selections were made, if more than one spin state was still possible, the spin value used in the calculation of the ^{26}Si(α,p) reaction rate was randomly chosen.

V. ASTROPHYSICAL IMPLICATIONS

For both ^{29}P(p,γ)^{30}S and ^{26}Si(α,p)^{29}P the reaction rates are dominated by the resonant reaction contributions due to the fairly large level density in the ^{30}S compound nucleus. In particular for radiative proton capture on ^{29}P it was demonstrated in earlier work [15, 16] that the direct-capture component in the reaction rate is negligible. We, therefore, concentrate in the following on the resonant contributions to the reaction rate.

The resonant reaction rate was calculated using the expression for narrow, well-separated resonances [38, 39]

$$N_A < \sigma v > = 1.54 \times 10^{11} A^{-3/2} T_9^{-3/2} \times \sum_i \omega\gamma_i \; exp\left(-\frac{11.605 E_i}{T_9}\right) \tag{6}$$

with A being the reduced mass (in atomic mass units), E_i the resonance energy in the center-of-mass system in MeV, and T_9 the temperature in units of GK. The resonance strength $\omega\gamma$ in MeV is defined as

$$\omega\gamma = \frac{2J+1}{(2I_1+1)(2I_2+1)} \times \frac{\Gamma_a\Gamma_b}{\Gamma} \tag{7}$$

In the case of the ^{26}Si(α,p)^{29}P reaction, J, $I_1 = I_\alpha = 0$, and $I_2 = I_{^{26}Si} = 0$ are the total angular momentum of the resonance, the α-particle, and the ^{26}Si, respectively. $\Gamma_a = \Gamma_\alpha$ is the width of the α particle, while $\Gamma_b = \Gamma_{p_{tot}} = \Gamma_p + \sum_i^7 \Gamma_{p^i}$ is the total proton-width and Γ is the total width of the state.

In the case of the ^{29}P(p,γ)^{30}S reaction, J, $I_1 = I_p = 1/2$ and $I_2 = I_{^{29}P} = 1/2$ are the total angular momentum of the resonance, the proton and the ^{29}P ground state, respectively. $\Gamma_a = \Gamma_{p_{tot}} = \Gamma_p + \sum_i^7 \Gamma_{p^i}$ is the total proton-width, $\Gamma_b = \Gamma_\gamma$ is the γ-width, and Γ is the total width of the state.

The partial widths were calculated using the formalism and the nuclear structure assumptions outlined in the previous section and listed in the Tables VI and VII. The resonance strengths were derived from these parameters. It should be noted that the nuclear structure input parameters carry a large uncertainty since they are not experimentally determined but are based on assumptions of typical single-particle and alpha-cluster strength distributions in this particular mass and excitation range of even-even nuclei. The classical approach is to weigh the uncertainty range for each resonance with a factor of (0-1) [38]. Empirically, we assume an uncertainty within one order of magnitude for the spectroscopic input parameters. Recently an attempt was made to provide an improved quantification of the uncertainty range based on Monte Carlo simulations assuming a characteristic Porter-Thomas distribution for the spectroscopic factors [40]. While this seems to be a reasonable approach for mid-shell nuclei, it is not necessarily a valid assumption for closed-shell even-even nuclei where the number of statistical configurations is limited and pronounced cluster configurations near the alpha threshold cannot be excluded. In view of the uncertainties associated with the single-particle and alpha-cluster configurations in ^{30}S we feel that the proposed Monte Carlo approach is insufficient to cover the potentially large uncertainty range of the estimate. In the following we discuss the rates and compare them with previous evaluations.

A. The ^{29}P(p,γ)^{30}S reaction rate

A total of 24 possible resonances listed in Table II have been included in the estimate of the ^{29}P(p,γ)^{30}S reaction rate but only the six states from 4.683 MeV to 5.382 MeV, shown in Fig. 8, contribute significantly to the reaction rate. All other contributions are small and fall within the hatched area shown in the figure. The resonance parameters are given in Table VI. The resonance strengths for the two states at 4.683 MeV and 4.814 MeV are determined by their proton-partial widths, which in turn depends on the single-particle spectroscopic factors adopted for these states [22]. For the higher-energy resonances the strength depends primarily on the gamma-decay strength which in most cases was adopted from the mirror levels in ^{30}Si. The resonance-reaction rates calculated in this work are compared to previous calculations in Fig. 9 where the rates are presented as ratios to the rate calculated by Iliadis *et al.* [16]. The rate predicted by the statistical model NON-SMOKER [41] is substantially larger than any of the rates based on experimental level information. Given the relatively limited level density in the ^{30}S compound nucleus below 9 MeV excitation energy, we rule out the statistical model as viable theoretical approach in this mass range. At higher temperatures all experiment based predictions are in reasonable agreement, they deviate toward lower temperatures. Early estimates by Wiescher & Görres (1987) [15], and Iliadis *et al.* (2001) [16] show the largest deviation from the present results which is due to uncertainties in the level structure in the compound nucleus ^{30}S, which handicapped their analysis. The later work of Bardayan *et al.* (2007) [10] and more recently by Setoodehnia *et al.* (2010) [22] shows good agreement within a factor of two, but is lower than the present prediction at temperatures T $\leq$ 0.25 GK. This is primarily due to the revised excitation energy of the lowest resonance state, which is also supported by the recent in-beam gamma-spectroscopy study by Setoodehnia *et al.* (2011) [35].

The total resonance-reaction rate calculated in the present work is shown in Table VIII in comparison with the resonance-reaction rate proposed by Iliadis *et al.* [16].

B. The ^{26}Si(α,p)^{29}P reaction rate

Present simulations of the αp-process rely on statistical model predictions for the ^{26}Si(α,p)^{29}P reaction rate. States in ^{30}S above the alpha threshold have not been observed prior to this work. Yet, the level structure and the level decay channels are not known and the derivation of the resonance strengths, therefore, carries large uncertainties.

TABLE VI. Resonance parameters used in the calculations of the ^{29}P(p,γ)^{30}S resonance reaction rate.

E_x MeV	E_{cm} MeV	J^π	C^2S	Γ_p eV	Γ_γ eV	$\omega\gamma$ MeV
4.6825	0.2835	3^+	0.04 [a]	0.000023 [a]	0.0049 [a]	4.01×10^{-11} [a]
4.814	0.4150	2^+	0.11 [a]	0.037 [a]	0.0048 [a]	2.61×10^{-9} [a]
5.130	0.7310	4^+	0.02	0.23	0.00793 [b]	1.72×10^{-8}
5.2178	0.8188	0^+	0.01	15.898	0.01115 [b]	2.79×10^{-9}
5.3121	0.9131	3^-	0.33	0.0033	0.01530 [b]	4.75×10^{-9}
5.382	0.9830	2^+	0.06	8.0436	0.31333 [b]	3.90×10^{-8}
5.8355	1.4365	4^+	0.001	0.00279	0.04387 [b]	5.90×10^{-9}
6.00	1.6010	0^+	0.56	74838	0.015	3.75×10^{-9}
6.24	1.8410	2^+	0.58	4647.54	0.039 [b]	4.84×10^{-8}
6.3259	1.9269	0^+	0.44	130000	0.082	2.05×10^{-8}
6.5121	2.1131	1^-	0.25	52241	0.047 [b]	3.52×10^{-8}
6.7375	2.3385	2^+	0.1	3489	0.0274	3.42×10^{-8}
6.9015	2.5025	1^-	0.1	45300	0.021	1.57×10^{-8}
7.0589	2.6599	0^+	0.1	106000	0.046	1.15×10^{-8}
7.1949	2.7959	3^-	0.1	2849	0.026	4.55×10^{-8}
7.3106	2.9116	2^+	0.1	21011	0.0387 [b]	4.84×10^{-8}
7.4465	3.0475	4^+	0.1	568	0.0548 [b]	1.12×10^{-7}
7.899	3.500	2^+ [c]	0.1	66872	0.582	7.27×10^{-7}
8.0828	3.6838	3^- [c]	0.1	32749	0.042	7.35×10^{-8}
8.4823	4.0833	1^- [c]	0.1	2670	0.127	9.52×10^{-8}
8.68	4.2810	4^+ [c]	0.1	13627	0.075	1.69×10^{-7}
8.875	4.4760	0^+ [c]	0.1	156800	0.166	4.15×10^{-8}
9.0806	4.6816	2^+ [c]	0.1	70700	0.186	2.32×10^{-7}
9.2763	4.8773	4^+ [c]	0.1	34258	0.114	2.56×10^{-7}

[a] From Setoodehnia *et al.* [22]
[b] Lifetimes from mirror states
[c] Spin randomly chosen among possible values.

We assume only a small alpha-cluster configuration represented by the spectroscopic factor C^2S_α=0.01. The single-particle strength of levels at this high excitation energy is also assumed to be lower and we adopted a single-particle spectroscopic factor C^2S_p=0.01. In all cases the alpha-partial width is considerably smaller than the proton-partial width and, therefore, determines the resonance strength distribution. In lighter T = 1 nuclei such as ^{18}O, ^{22}Ne and ^{26}Mg, pronounced α-cluster configurations above the alpha-decay threshold have been observed [42–48]. Therefore, the possibility of much higher resonance strengths cannot be excluded. A total of 25 resonances were considered for contributing to the reaction rate of ^{26}Si(α,p)^{29}P. The resonance parameters are given in Table VII. The spin of the resonances were randomly chosen among the possible values as discussed in Section IV D. To estimate the uncertainty in this random approach, the reaction rate was calculated using a different set of spins. We found that the ^{26}Si(α,p)^{29}P reaction rate varies up to a factor of 10 when a different set of spins is chosen.

Many resonances contribute to the total reaction rate shown in Fig. 10. The figure also shows the reaction rates calculated using the statistical models SMOKER [49], NON-SMOKER [50], TALYS [51] and CIGAR [52] which are typically used to calculate this reaction rate.

The Hauser-Feshbach rates agree with each other within less than an order of magnitude, depending on the specific treatment for excitation energy and deformation dependence of level densities. The reaction rates predicted by the different Hauser-Feshbach calculations are listed in Table VIII in comparison with the rates predicted on the basis of the experimental data.

All of the statistical rates are substantially larger than the rate based on the observed resonance structure. Using the code CIGAR [52] we examined the sensitivity of the calculated reaction rate to both the radius and diffuseness of the real and imaginary components of the alpha optical potential model. We find that increasing the real and imaginary radius and diffuseness by a factor of 1.086 reduces the reaction rate by up to a factor of ~ 3. This result highlights the critical need for a better understanding of the alpha optical potential.

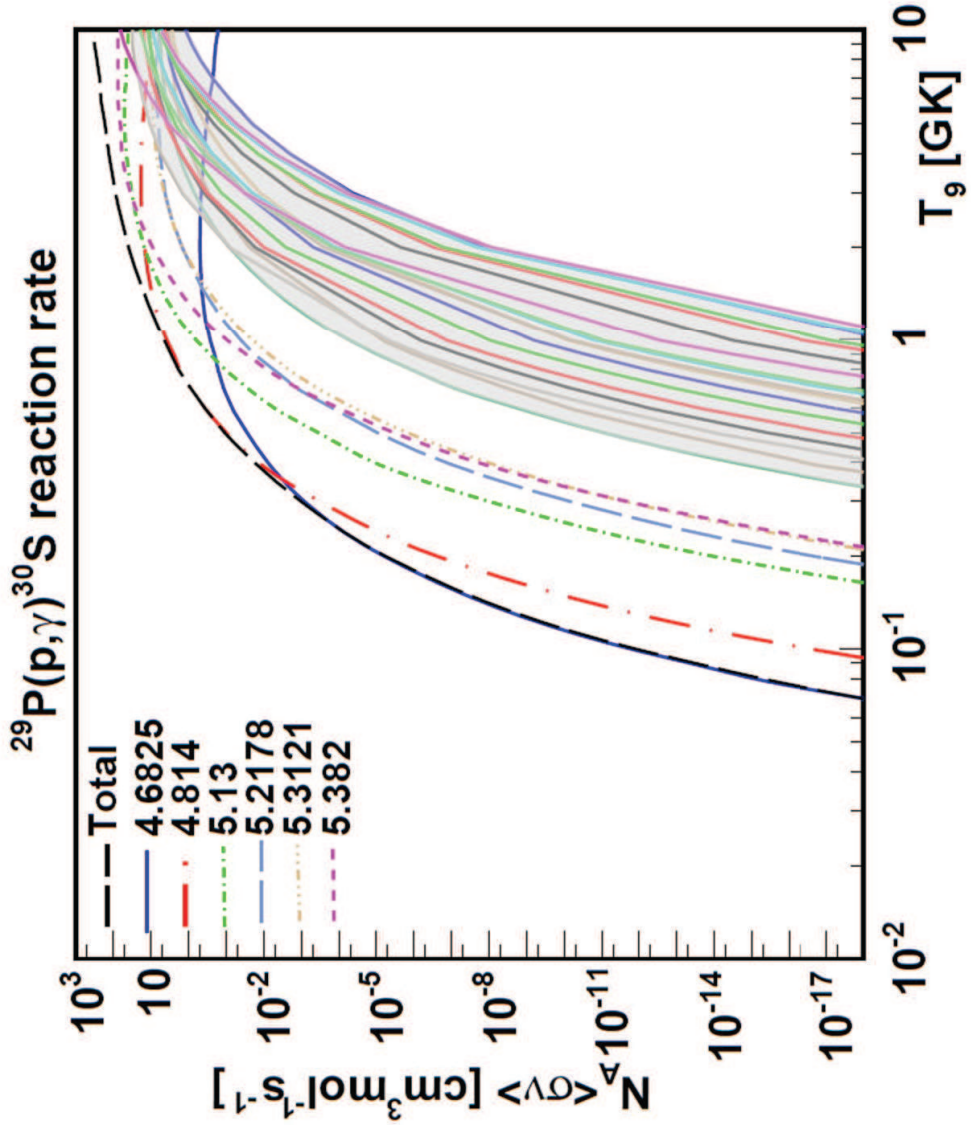

FIG. 8. (Color online) Contribution of the most relevant resonances to the ^{29}P(p,γ)^{30}S reaction rate. All other resonances listed in Table VI fall within the shadowed area and have a limited contribution to the reaction rate.

The reaction rate scales directly with the resonance strengths which in turn depend on the α-strengths. We have tested the impact of possible alpha-cluster states near the alpha threshold by increasing the strengths of resonances inside the Gamov window by two orders of magnitude. This causes an enhancement in a relative narrow temperature range corresponding to the excitation energy of the resonance level, but has limited effect on the overall reaction rate over the entire temperature range. It is clear that the question of the α-strength distribution in this excitation energy range and its impact on the reaction rate require more detailed studies of the ^{30}S compound nucleus at higher energies.

VI. CONCLUSIONS

The present work was focused on the nuclear level structure in ^{30}S and the consequences for the resonant contributions to the reaction cross-sections of the ^{29}P(p,γ)^{30}S radiative capture and the ^{26}Si(α,p)^{29}P nuclear reaction process. Both reactions play a key role in the *rp*-process and the αp-process in explosive hydrogen burning [9, 14]. The experiments helped to improve existing information on previously observed levels but in addition a large number

TABLE VII. Resonance parameters used in the calculations of the ^{26}Si(α,p)^{29}P resonance reaction rate.

E_x	E_{cm}	J^π [a]	$C^2S(\alpha)$	Γ_α	$C^2S(p)$	Γ_p	$\omega\gamma$
MeV	MeV			eV		eV	MeV
9.3914	0.0484	2^+	0.01	9.78×10^{-89}	0.01	9200	4.89×10^{-94}
9.486	0.1430	1^-	0.01	2.87×10^{-45}	0.01	44500	8.61×10^{-51}
9.7012	0.3582	2^+	0.01	3.30×10^{-24}	0.01	12357	1.65×10^{-29}
9.7851	0.4421	0^+	0.01	1.38×10^{-19}	0.01	444962	1.38×10^{-25}
9.8742	0.5312	2^+	0.01	2.00×10^{-17}	0.01	14126	1.00×10^{-22}
10.0088	0.6658	4^+	0.01	3.90×10^{-16}	0.01	758.11	2.61×10^{-21}
10.0705	0.7275	0^+	0.01	3.24×10^{-12}	0.01	131513	3.24×10^{-18}
10.1226	0.7796	4^+	0.01	3.59×10^{-14}	0.01	844.87	3.23×10^{-19}
10.2747	0.9317	2^+	0.01	4.63×10^{-10}	0.01	18166	2.32×10^{-15}
10.4431	1.1001	3^-	0.01	6.28×10^{-9}	0.01	3975	4.40×10^{-14}
10.65	1.307	3^-	0.01	3.53×10^{-7}	0.01	4630	2.47×10^{-12}
10.7551	1.4121	3^-	0.01	1.92×10^{-6}	0.01	4990	1.35×10^{-11}
10.8149	1.4719	4^+	0.01	3.13×10^{-7}	0.01	1545	2.82×10^{-12}
11.0154	1.6724	4^+	0.01	4.41×10^{-6}	0.01	1812	3.97×10^{-11}
11.10	1.757	3^-	0.01	1.62×10^{-4}	0.01	6296	1.14×10^{-9}
11.20	1.857	3^-	0.01	4.61×10^{-4}	0.01	6708	3.23×10^{-9}
11.30	1.957	4^+	0.01	9.18×10^{-5}	0.01	2250	8.26×10^{-10}
11.3997	2.0567	4^+	0.01	2.28×10^{-4}	0.01	2421	2.05×10^{-9}
11.4904	2.1474	4^+	0.01	4.94×10^{-4}	0.01	2586	4.45×10^{-9}
11.5462	2.2032	1^-	0.01	1.59×10^{-1}	0.01	3964	4.77×10^{-7}
11.6091	2.2661	4^+	0.01	1.27×10^{-3}	0.01	2813	1.14×10^{-8}
11.6817	2.3387	3^-	0.01	2.60×10^{-2}	0.01	8854	1.82×10^{-7}
11.77	2.427	4^+	0.01	4.05×10^{-3}	0.01	3146	3.64×10^{-8}
11.8523	2.5093	3^-	0.01	8.07×10^{-2}	0.01	9660	5.65×10^{-7}
12.0392	2.6962	0^+	0.01	4.84×10^{0}	0.01	24889	4.84×10^{-6}

[a] Spin randomly chosen among possible values.

of levels up to high excitation energies have been observed for the first time. The high resolution of the Grand Raiden spectrometer reduced substantially the uncertainty in the excitation and resonance energies of the populated states, removing one of the main handicaps for determining accurate reaction rates. The proton-decay studies provided additional information and constraint for the spin-parity assignments of the observed states. The reaction-rate calculation requires detailed information about the specific partial widths of the contributing resonance levels, namely the proton-partial widths of the low-energy resonances in ^{29}P(p,γ)^{30}S and the alpha-partial widths of the resonances in ^{26}Si(α,p)^{29}P. These parameters are based on empirical quasi-statistical assumptions about the single-particle and the alpha-cluster strength distribution in ^{30}S. While strong single-resonance contributions from pronounced single-particle states or cluster configurations cannot be excluded, the high resonance density reduces the overall impact of such pronounced resonance structures on the reaction rate.

ACKNOWLEDGMENTS

The authors are grateful for the support and help by the technical staff of the Notre Dame Nuclear Science Laboratory and the RCNP cyclotron facility at Osaka, Japan during the course of the experiments. This work was supported by the NSF through grants PHY0822648, PHY0758100, U. S. Department of Energy through grants DE-FG02-88ER40387 and DE-FG52-09NA29455 and JINA PHY1068192.

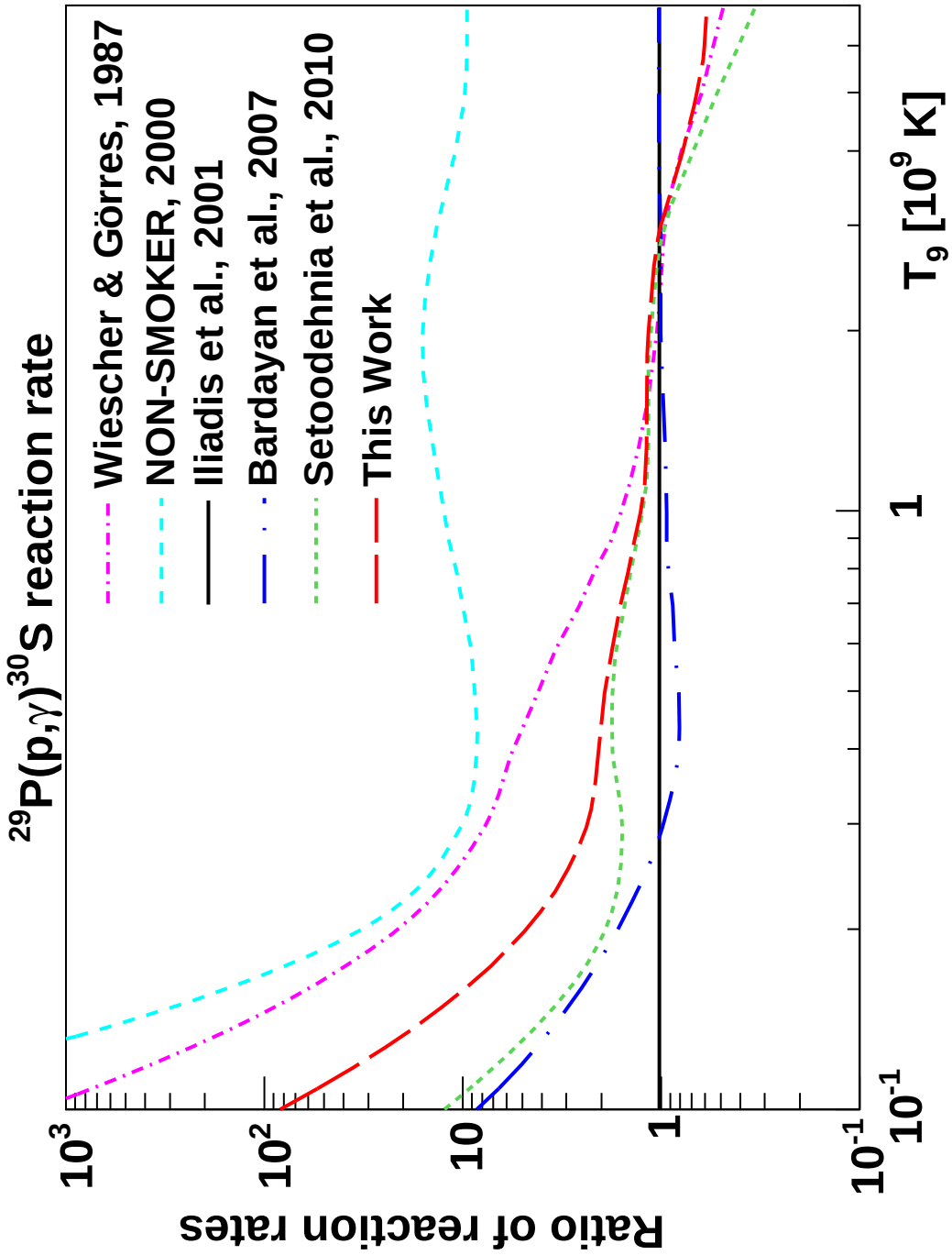

FIG. 9. (Color online) Resonance contribution to the ^{29}P(p,γ)^{30}S reaction rate calculated in this work and comparison with previous works. The reaction rates are plotted as ratios to the rate calculated by Iliadis *et al.* [16].

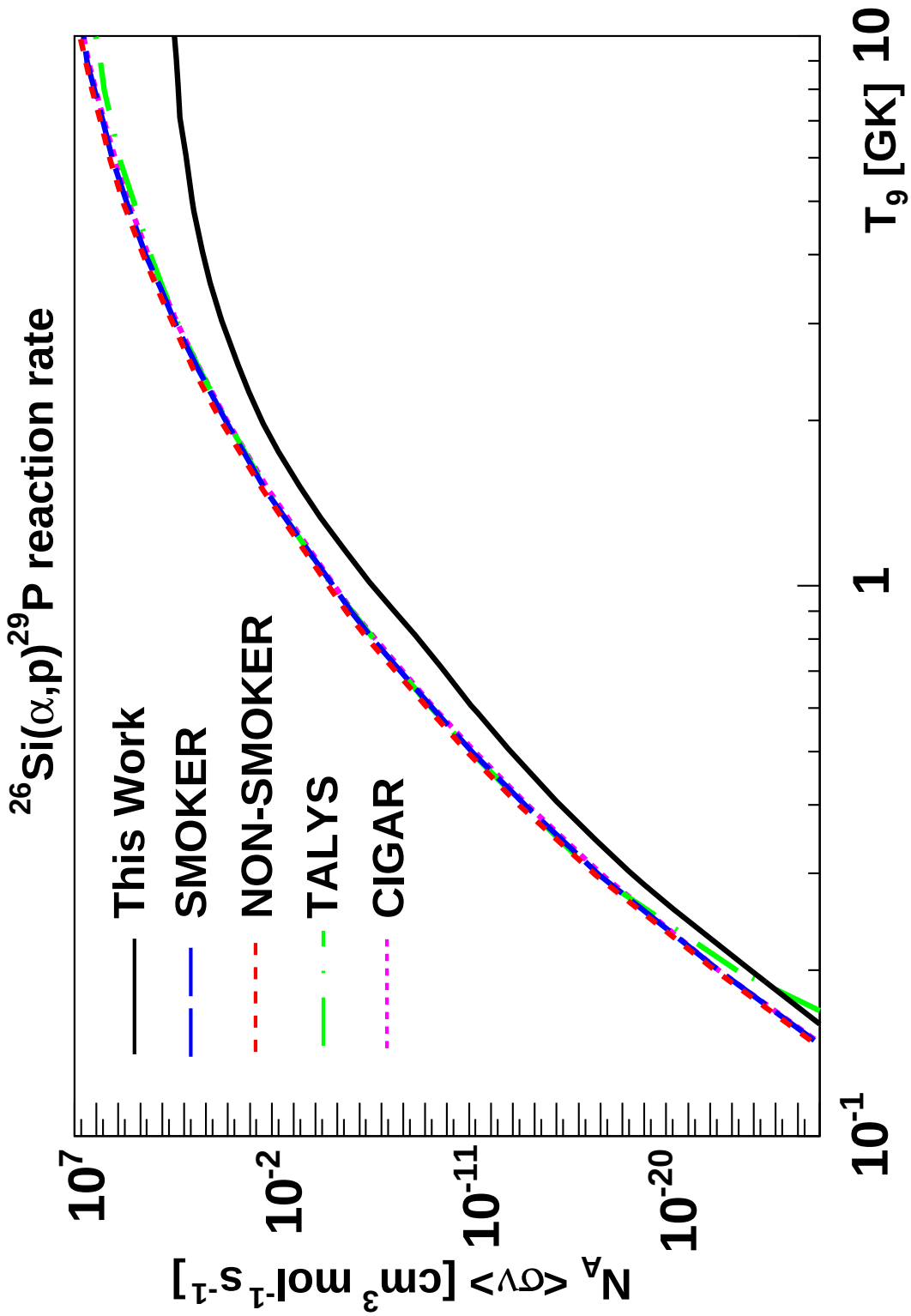

FIG. 10. (Color online) Resonance contribution to the ^{26}Si(α,p)^{29}P reaction rate calculated using the parameters given in Table VII and comparison with the rates calculated using the statistical codes SMOKER [49], NON-SMOKER [50], TALYS [51] and CIGAR [52].

TABLE VIII. ^{29}P(p,γ)^{30}S and ^{26}Si(α,p)^{29}P resonance reaction rates calculated in this work and comparison with previous calculations.

	^{29}P(p,γ)^{30}S reaction rate		^{26}Si(α,p)^{29}P reaction rate				
T_9	This Work	Iliadis *et al.* [16]	This Work	SMOKER [49]	NON-SMOKER [50]	TALYS [51]	CIGAR [52]
0.1	1.06E-12	1.27E-14	1.66E-35	1.09E-34	2.93E-34		1.08E-34
0.15	3.34E-08	2.71E-09	1.44E-28	1.38E-27	2.30E-27	1.24E-30	1.47E-27
0.2	5.37E-06	1.11E-06	1.78E-24	3.26E-23	5.05E-23	4.36E-24	3.18E-23
0.25	1.15E-04	3.85E-05	1.84E-21	3.88E-20	6.14E-20	3.43E-20	
0.3	9.57E-04	4.04E-03	3.83E-19	8.36E-18	1.37E-17	1.30E-17	7.28E-18
0.35	4.75E-03	2.20E-03	2.40E-17	6.02E-16	1.02E-15		
0.4	1.68E-02	8.13E-03	6.81E-16	2.04E-14	3.56E-14	2.50E-14	1.64E-14
0.5	1.04E-01	5.47E-02	1.15E-13	5.13E-12	9.35E-12	5.76E-12	4.61E-12
0.6	3.60E-01	2.08E-01	5.72E-12	3.45E-10	6.43E-10	4.15E-10	3.35E-10
0.7	8.72E-01	5.58E-01	1.41E-10	9.85E-09	1.86E-08	1.18E-08	9.85E-09
0.8	1.69E+00	1.18E+00	2.21E-09	1.56E-07	2.95E-07	1.81E-07	1.56E-07
0.9	2.85E+00	2.14E+00	2.57E-08	1.59E-06	3.01E-06	1.81E-06	1.60E-06
1.0	4.37E+00	3.47E+01	2.32E-07	1.17E-05	2.21E-05	1.31E-05	1.17E-05
1.5	1.75E+01	1.53E+01	4.25E-04	1.25E-02	2.28E-02	1.28E-02	1.22E-02
2.0	3.85E+01	3.37E+01	2.38E-02	9.15E-01	1.61E+00	8.68E-01	8.96E-01
2.5	6.28E+01	5.74E+01	2.75E-01	1.79E+01	3.06E+01	1.58E+01	1.77E+01
3.0	8.68E+01	8.76E+01	1.40E+00	1.63E+02	2.71E+02	1.34E+02	1.63E+02
3.5	1.09E+02	1.24E+02	4.39E+00	9.09E+02	1.47E+03	6.96E+02	9.16E+02
4.0	1.29E+02	1.66D+02	1.02E+01	3.60E+03	5.67E+03	2.56E+03	3.64E+03
5.0	1.64E+02	2.53E+02	3.18E+01	2.89E+04	4.34E+04	1.76E+04	2.91E+04
6.0	1.97E+02	3.33E+02	6.52E+01	1.30E+05	1.88E+05	6.69E+04	1.29E+05
7.0	2.31E+02	3.98E+02	1.05E+02	4.04E+05	5.66E+05	1.76E+05	3.99E+05
8.0	2.66E+02	4.47E+02	1.47E+02	9.77E+05	1.34E+06	3.59E+05	9.62E+05
9.0	3.00E+02	4.81E+02	1.87E+02	1.97E+06	2.70E+06	6.18E+05	1.96E+06
10.0	3.34E+02	5.03E+02	2.23E+02	3.47E+06	4.83E+06	9.37E+05	3.50E+06

[1] R. K. Wallace and S. E. Woosley, *Astrophys. J. Suppl. Ser.* **45**, 389 (1981).
[2] L. Van Wormer et al., *Ap. J.* **432**, 326 (1994).
[3] H. Schatz et al., *Phys. Rev. Lett.* **79**:20, 3845 (1997).
[4] S. Starrfield et al., *Nucl. Phys. A* **621**, 495 (1997).
[5] M. Wiescher, J. Görres, F.-K. Thielemann and H. Ritter. *A&A* **160**, 56 (1986).
[6] C. Iliadis, A. E. Champagne, J. José, S. Starrfield and P. Tupper, *Astrophys. J. Suppl. Ser.* **14. Görres2**, 105 (2002).
[7] E. Zinner, *Annu. Rev. Earth Planet Sci.* **26**, 147 (1998).
[8] S. Amari, X. Gao, L. R. Nittler, E. Zinner, J. Jose, M. Hernanz and R. S. Lewis, *Astrophys. J.* **551**, 1065 (2001).
[9] J. José, M. Hernanz, S. Amari, K. Lodders and E. Zinner, *Astrophys. J.* **612**, 414 (2004).
[10] D. W. Bardayan, et al., *Phys. Rev. C* **76**, 045803 (2007).
[11] M. Sztajno et al., *Astrophys. J.* **299**, 487 (1985).
[12] W. Penninx, E. Damen, J. Van Paradijs and W. H. G. Lewin, *A&A* **208**, 146 (1989).
[13] E. Kuulkers et. al., *A&A* **382**, 947 (2002).
[14] J. L. Fisker, F.-K. Thielemann and M. Wiescher, *Astrophys. J.* **608**, L61 (2004).
[15] M. Wiescher and J. G*örres*, *Z. Phys. A*, **329**, 121 (1987).
[16] C. Iliadis, J. M. D'Auria, S. Starrfield, W. J. Thompson, and M. Wiescher, *Astrophys. J. Suppl. Ser.* **134**, 151 (2001).
[17] R. A. Paddock, *Phys. Rev. C* **5**, 485 (1972).
[18] J. M. G. Caraça, R. D. Gill, A. J. Cox and H. J. Tose, *Nucl. Phys. A* **193**, 1 (1972).
[19] E. Kuhlmann, W. Albrecht and A. Hoffmann, *Nucl. Phys. A* **213**, 82 (1973).
[20] H. Yokota, K. Fujioka, K. Ichimaru, Y. Mihara and R. Chiba, *Nucl. Phys. A* **383**, 298 (1982).
[21] H. O. U. Fynbo et al., *Nucl. Phys. A* **677**, 38 (2000).
[22] K. Setoodehnia, et al., *Phys. Rev. C* **82**, 022801(R) (2010).
[23] A. Matic et al., *Phys. Rev. C* **84**, 025801 (2011).
[24] A. Matic et al., *Phys. Rev. C* **80**, 055804 (2009).
[25] A. Matic et al., *Phys. Rev. C* **82**, 025807 (2010).
[26] G. Audi, O. Bersillon, J. Blachot, A.H. Wapstra, *Nucl. Phys. A* **729**, 3 (2003).
[27] J. Souin, T. Eronen, P. Ascher, L. Audirac, J. Äystö, B. Blank, V.-V. Elomaa, J. Giovinazzo, J. Hakala, A. Jokinen, V. S. Kolhinen, P. Karvonen, I.D. Moore, S. Rahaman, J. Rissanen, A. Saastamoinen, and J. C Thomas, *Eur. Phys. J. A* **47**, 40 (2011).
[28] M. Fujiwara et al., *Nucl. Inst. Meth. Phys. Res. A* **422**, 484 (1999).
[29] T. Wakasa et al., *Nucl. Inst. Meth. Phys. Res. A* **482**, 79 (2002).
[30] W. P. Tan, J. L. Fisker, J. Görres, M. Couder and M. Wiescher, *Phys. Rev. Lett.* **98**, 242503 (2007).
[31] W. P. Tan et. al., *Phys. Rev. C* **79**, 055805 (2009).
[32] W. R. Leo, *Techniques for Nuclear and Particle Physics Experiments*, Springer-Verlag (1994).
[33] *MPD-4*, www.mesytec.com/datasheets/MPD-4.pdf.
[34] C. Iliadis, *Nucl. Phys. A* **618**, 166 (1997).
[35] K. Setoodehnia, et al., *Phys. Rev. C* **83**, 018803(R) (2011).
[36] P. D. Kunz, *DWUCK4 code*, Unpublished.
[37] P. Mohr, *Phys. Rev. C* **61**, 045802 (2000).
[38] W. A. Fowler, G. R. Caughlan, B. A. Zimmerman, *Ann. Rev. Nucl. Part. Sci.* **13**, 69 (1975)
[39] C. E. Rolfs and W. S Rodney, *Cauldrons in the Cosmos*, The University of Chicago Press (1998).
[40] C. Iliadis, R. Longland, A. E. Champagne, A. Coc, *Nucl. Phys. A* **841**, 251 (2010).
[41] T. Rauscher and F - K Thielemann, *ADNDT* **75**, 1 (2000).
[42] V. Z. Goldberg et al. *Phys. Atom. Nucl.* **68**, 1079 (2005).
[43] J. Görres et al. *Nucl. Phys. A* **548**, 414 (1992).
[44] V. Z. Goldberg et al. *Phys. Rev. C* **69**, 24602 (2004).
[45] H.-P. Trautvetter et al. *Nucl. PHys. A* **297**, 489 (1978).
[46] B. L. Berman, R. L. van Hemert and C. D. Bowman *Phys. Rev. Lett* **23**, 386 (1996).
[47] F. Kaeppeler et al. *Astrophys. J.* **437**, 396 (1994).
[48] T. Rauscher, F.-K. Thielemann, J. Görres and M. Wiescher *Nucl. Phys. A* **675**, 695 (2000).
[49] F - K. Thielemann, et al. *Adv. Nucl. Astro.*, **525** (1987). *http* : *//ie.lbl.gov/astro2/rate5.text.*
[50] R. H. Cyburt et al. *ApJS*, **189**, 240 (2010) T. Rauscher REACLIB.
[51] A.J. Koning, S. Hilaire and M.C. Duijvestijn, "TALYS-1.0", *Proceedings of the International Conference on Nuclear Data for Science and Technology, April 22-27, 2007, Nice, France, editors O.Bersillon, F.Gunsing, E.Bauge, R.Jacqmin, and S.Leray, EDP Sciences*, p. 211(2008).
[52] A. Palumbo et al. *Phys. Rev. C* (2012) submitted.